DISSERTATIONES
PHYSICAE
UNIVERSITATIS
TARTUENSIS
122

KALEV ERME

The effect of catalysts in plasma oxidation of nitrogen oxides

DISSERTATIONES PHYSICAE UNIVERSITATIS TARTUENSIS
122

DISSERTATIONES PHYSICAE UNIVERSITATIS TARTUENSIS
122

KALEV ERME

The effect of catalysts in plasma oxidation of nitrogen oxides

UNIVERSITY OF TARTU
Press

Institute of Physics, Faculty of Science and Technology, University of Tartu.

The dissertation was admitted on June 11, 2019 in partial fulfillment of the requirements for the degree of Doctor of Philosophy in Physics, and was allowed for defense by the Council of the Institute of Physics, University of Tartu.

Supervisor: PhD Indrek Jõgi, University of Tartu

Opponent: Assoc. Prof. Joanna Pawlat, Lublin University of Technology, Lublin, Poland

Defense: September 6, 2019 at the University of Tartu

This work has been partially supported by Graduate School of Functional Materials and Technologies receiving funding from the European Regional Development Fund in University of Tartu, Estonia.

ISSN 1406-0647
ISBN 978-9949-03-089-7 (print)
ISBN 978-9949-03-090-3 (pdf)

University of Tartu Press
www.tyk.ee

TABLE OF CONTENTS

LIST OF ORIGINAL PUBLICATIONS

I I. Jõgi, **K. Erme**, A. Haljaste, M. Laan, Oxidation of nitrogen oxide in hybrid plasma-catalytic reactors based on DBD and Fe_2O_3, *The European Physical Journal: Applied Physics* 61 (2013) 24305.

II I. Jõgi, **K. Erme**, J. Raud, M. Laan, Oxidation of NO by ozone in the presence of TiO_2 catalyst, *Fuel* 173 (2016) 45–51.

III **K. Erme**, J. Raud, I. Jõgi, Adsorption of Nitrogen Oxides on TiO_2 Surface as a Function of NO_2 and N_2O_5 Fraction in the Gas Phase, *Langmuir* 34 (2018) 6338–6345.

IV I. Jõgi, **K. Erme**, E. Levoll, J. Raud, E. Stamate, Plasma and catalyst for the oxidation of NO_x, *Plasma Sources Science and Technology* 27 (2018) 35001.

V **K. Erme**, I. Jõgi, Metal Oxides as Catalysts and Adsorbents in Ozone Oxidation of NO_x, *Environmental Science & Technology* 53 (2019) 5266−5271.

Author's contribution

Paper I: participation in experimental work.

Paper II: performing the experiments and most of data analysis.

Paper III: performing most of the experiments; data analysis, manuscript preparation.

Paper IV: participation in experimental work and data analysis.

Paper V: performing the experiments, data analysis and manuscript preparation.

ABBREVIATIONS

SNCR	selective non-catalytic reduction
SCR	selective catalytic reduction
NSR	NO_x storage reduction
NTP	non-thermal plasma
DBD	dielectric barrier discharge
VOC	volatile organic compounds
DRIFTS	diffuse reflectance infrared Fourier transform spectroscopy
SIE	specific input energy
TPD	temperature programmed desorption
XPS	X-ray photoelectron spectroscopy

1. INTRODUCTION

A growing problem in densely populated areas is atmospheric pollution. Among various gaseous pollutants, nitrogen oxides NO and NO_2, commonly labelled by the term NO_x, are subject to increasingly strict regulations because of their detrimental effect on the environment. Created primarily in fuel combustion processes and exiting into the atmosphere, they can be the precursors of acid rain and smog and have adverse health effects on the population [1–5]. For this reason it is important to develop different methods of NO_x removal from exhaust gases.

The main conventional methods for NO_x removal are scrubbing, selective catalytic reduction (SCR) and NO_x storage reduction (NSR). In scrubbing, NO_x gases are absorbed in liquid solutions, in which they form salts and nitrogen acids. In SCR, the NO_x species are reduced on the surface of a catalyst in the presence of certain reducing agents [4]. In NSR, NO_x gases are removed in a cyclic operation: the initial step of adsorption onto a surface is followed by a change in gas composition, which in turn induces reduction of the adsorbed species [6]. These methods suffer from poor absorption and adsorption of NO, which generally constitute the majority among NO_x emissions [2, 3]. Therefore, oxidation of NO to NO_2 is necessary to improve NO_x removal.

Non-thermal plasma (NTP) can be applied for the oxidation of NO_x because of its property to produce highly oxidizing species, such as O and OH radicals and ozone [7–9]. NTP enables the process to be carried out at low temperatures and has the possibility of fast adaptation to quickly changing gas composition. The method can also be combined with the usage of catalysts to further improve oxidation efficiency, which has been shown in several previous studies [10–13]. A potentially suitable class of materials for this purpose is metal oxides, which can function both as catalysts and adsorbents. In scientific literature, direct adsorption of NO_x on the surfaces of metal oxides has been studied, along with surface reaction pathways [14–19]. However, in the presence of plasma-generated active species the surface processes are less clear.

In the present thesis, the role of metal oxide powders was investigated in the oxidation of NO_x by plasma-generated species. Studies were carried out to construct mathematical models describing the removal processes in both single-stage and two-stage catalyst placement configurations. The influence of TiO_2, γ-Al_2O_3 and γ-Fe_2O_3 were compared in the case of NO_x oxidation in the two-stage system. Additional experimental and data analysis techniques were applied to clarify the processes taking place on the surfaces of the metal oxide powders during the oxidation process.

In the structure of the current thesis, the following major parts can be highlighted. In chapter 2, an overview is given on the basis of scientific literature, summarizing the main aspects of NO_x sources and adverse effects, conventional methods of their removal and the main aspects of removal methods with plasma and catalyst. In chapter 4, details concerning experimental

equipment and measurement methods are provided. The first part of chapter 5 deals with the oxidation of NO_x directly by plasma and the effect of catalyst in the single-stage configuration. In section 5.2, the efficiency of indirect plasma oxidation of NO_x is analyzed. Section 5.3 is devoted to in-depth analysis of the collected data and additional measurements for the purpose of constructing models for surface processes.

2. SCIENTIFIC BACKGROUND

2.1. Sources and adverse effects of NO_x

NO_x is a generic term that is usually assigned to the gases NO and NO_2. Among nitrogen oxides, these compounds are the most relevant to atmospheric pollution.

NO_x compounds are mainly formed by reactions between nitrogen and oxygen at high temperatures. For this reason, the most important sources of NO_x involve fuel combustion – motor vehicles, industrial power plants and technologies, etc. Diesel engines, for example, are problematic in this regard, especially those of marine vessels, which can produce NO_x emissions up to 1300 ppm [1]. Although the ratio of emitted NO and NO_2 may vary, depending on the conditions of operation, NO constitutes a large majority (above 90%) in primary NO_x emissions [2, 3].

Other sources of NO_x are less relevant to the current thesis but nevertheless worth mentioning. Processes related to agriculture may also cause NO_x emissions though the production of fertilizers and the use of nitrogen fixing plants [20, 21]. Among non-anthropogenic sources the most noteworthy is lightning, in which rapid heating and cooling processes emulate conditions similar to high-temperature fuel combustion, producing significant quantities of NO from N_2 and O_2 [22].

NO and especially NO_2 are toxic to humans. They can cause eye and throat irritation, lung injury, respiratory and cardiovascular diseases [4, 5]. In addition, NO_x have a number of indirect adverse effects. Upon reaching the atmosphere, NO slowly oxidizes to NO_2, which can in turn react with water vapor to form nitrogen acid HNO_3. The latter, together with sulfuric acid H_2SO_4, is an important component of acid rain and smog. Acid rains have a significant effect on soil and streamwater chemistry through large quantities of calcium and magnesium being lost from the soil complex and exported by drainage water. Acidification of soils in turn have adverse effects on forest ecosystems. Lowering of pH in surface waters can also cause the reduction of biodiversity in lakes and rivers. Acid rains can also damage buildings and monuments, made of limestone and marble, which contain large amounts of calcium carbonate [23]. Additionally, NO_x can react with various organic compounds to generate harmful products, such as ozone, nitroarenes, nitrosamines, nitrate radicals and nitryl chloride [24].

Due to the impact of NO_x on the environment and public health, increasingly strict regulations have been implemented to their emission from fuel combustion. For example, mobile sources in the European Union have the limits of 60–82 mg/km for petrol and 80–125 mg/km for diesel vehicles [25]. Combustion plant emissions must adhere to 50–225 ppm [26] and marine diesel engines to 2–3.4 g/kWh [27]. The specific limits within these ranges depend on the size of vehicle or plant.

2.2. Conventional methods for NO_x removal

Several methods have been developed that involve the reduction of NO_x to N_2 and O_2 (or H_2O). One such process, which has also been applied in practice, is selective non-catalytic reduction (SNCR). In this method, ammonia (NH_3) or urea (a.k.a. carbamide, NH_2CONH_2) is injected into the appropriate location of the burner outlet to react with NO_x that is formed in fuel combustion. The products of the redox reaction are N_2 and H_2O (and CO_2 in case of urea). The main drawback of the method is that it is only effective at high temperatures, in a limited range around 1000 °C. This in turn introduces complications related to mixing, as the reacting agents must efficiently reach high-temperature regions to avoid NO_x slip [28].

In selective catalytic reduction (SCR), ammonia or urea are used as reducing agents, but a catalyst is used to enable the NO_x removal process to proceed at lower temperatures, typically in the range 300–800 K. The catalysts are usually materials enhanced by noble metals (e.g. Pt/Al_2O_3), base metal oxides (e.g. those containing vanadium) or zeolites (e.g. Cu-ZSM-5). Compared to SNCR, SCR reduces energy consumption due to lower temperatures and can remove over 90% of NO_x, making it thus far the most popular NO_x control method. On the other hand, the use of catalyst introduces its own problems like surface poisoning and limited catalyst lifetime, as well as extra costs related to the applied materials [4].

NO_x storage reduction (NSR) is based on cyclic operation in which NO_x is alternately stored on a surface and reduced. The catalyst traps NO_x in lean-burn conditions in a process, which involves oxidation of NO to NO_2 and adsorption of NO_2. Before the maximum adsorption capacity is reached, the catalyst is exposed to a rich environment of the exhaust, which induces the release of NO_x from the surface and its reduction to N_2. NSR catalysts typically include alkali or alkaline-earth and precious metals, the most common composition being Pt and Ba supported on γ-Al_2O_3. The method has proven to be challenging in its complexity, stemming from the cyclic and transient nature of the process, mutual dependence of different steps, the existence of various deactivation mechanisms, etc. [6]

Removal of NO_x by absorption can be achieved by the use of scrubbing solutions, which have been applied in the chemical industry. Nitrites and nitrates are produced in case of alkaline solutions, whereas nitric and nitrous oxides are formed in case of water. As a drawback, HNO_2 is formed, which can decompose and result in reproduction of NO. Furthermore, the removal of NO suffers from poor absorption and would need to be oxidized to NO_2 [4].

The methods described above have undergone extensive research and development and have been put to use in various applications. Nevertheless, they exhibit certain downsides, e.g. related to either high energy consumption (SNCR) or cost of catalysts (SCR, NSR). There is also the issue of low flexibility in reacting to fast-changing gas composition and the need to regenerate catalyst surfaces. Given the abundance of NO within NO_x, the

difficulties of direct NO removal presents itself as a problem and the oxidation of NO to NO_2 is often necessary.

2.3. Removal by oxidation in plasma devices

Non-thermal plasma (NTP) can be applied for the purpose of gaseous pollutant removal, utilizing its property to produce active radicals like O, N or OH, which in turn can oxidize the pollutant species. The efficiency of NTP stems from selective transfer of energy to relevant processes without heating the gas. Another advantage of plasma treatment is its possibility of fast adaptation to quickly changing conditions and gas composition. In addition, it is possible to combine removal by NTP with other methods described above to mutually improve their respective performances.

NTP at atmospheric pressure for the purpose of pollutant removal can be produced by various techniques and experimental devices. These include dielectric barrier discharge (DBD), corona discharge, packed-bed and surface discharge reactors, characterized by the formation of streamers and micro-discharges. Microwave, radio frequency and gliding arc discharges have also been investigated for the use of gas processing [29–31]. These devices use pulsed or AC power supply and their performance can be controlled by the input power, frequency and pulse shape [32].

In case of pollutant removal, investigations have mostly focused on DBD, corona and packed-bed reactors. In the context of the current work, DBD is of the main interest. In this method, high AC voltage is applied to a small discharge gap which includes a dielectric barrier to separate the electrodes. In atmospheric pressure and especially in the presence of oxygen, formation of microdischarge channels takes place. The role of the dielectric barrier is to terminate the microdischarges before their increasing temperature leads to the development of arc discharge. Additionally, the charging of the dielectric enables the estimation of input energy during a period of applied voltage waveform [33, 34].

Since the concentration of NO in exhaust gas is relatively low, its direct dissociation by electron impact is not the primary mechanism of removal. Instead, the kinetic energy of electrons is deposited mainly into N_2 and O_2. From the point of view of NO_x removal, the most important processes associated with this energy are the dissociation reactions [7]

$$e + N_2 \rightarrow e + N + N,$$

$$e + O_2 \rightarrow e + O + O.$$

In the presence of H_2O, electron impact or reaction with metastable O-radical can also produce OH-radicals. The most useful are the oxygen radicals because

of their ability to oxidize NO to NO_2. Their production can consume up to 30% of the input energy [8].

An additional important process is the reaction of the O-radicals with O_2 to produce ozone:

$$O + O_2 + M \rightarrow O_3 + M.$$

Both O and O_3 are able to oxidize NO to NO_2, whereas O_3 can additionally oxidize NO_2 further to N_2O_5. While O_3 is relatively stable at room temperature, the lifetime of O is less than 100 μs [9], which prevents it from exiting the plasma reactor. This fact leads to the distinction of two different configurations of NO_x removal systems, based on NTP. In direct oxidation by plasma, the polluted gas stream is directed through the plasma reactor and both O and O_3 participate in the oxidation of NO_x. In indirect plasma oxidation, the exhaust is directed through a separate reaction chamber with an additional input from the plasma reactor, leaving O_3 the only oxidizing agent.

2.4. Pollutant removal by plasma-catalytic systems

Despite its advantages, pollutant removal by NTP, either directly or indirectly, also has its downsides. For example, high values of input energy may be needed in case of slowly progressing oxidation reactions, such as the oxidation of NO_2 to N_2O_5. Additionally, a potential problem is presented by ozone that is created in the plasma and that can subsequently exit the reactor, causing secondary pollution. Improvement of the beneficial oxidation reactions, as well as limiting the emission of O_3, can be achieved by combining NTP with the usage of solid-state catalysts.

The catalyst can be placed either between the electrodes in a DBD reactor, which is referred to as the single-stage configuration, or into a separate chamber downstream, which is called the two-stage configuration. The catalyst is usually in the form of a powder and there are several techniques of its placement. For example, in a packed-bed reactor, the powder fills the void between the pellets [10]. Ceramic foams and honeycombs include microporous channels, which facilitate the formation of surface microdischarges [11, 12].

The mutual interaction between plasma and catalyst is most complicated in the single-stage configuration. The modification of the catalyst surface by plasma mainly includes processes related to adsorption, but also local temperature increase and photocatalysis. Species created in plasma above the catalyst surface can adsorb and subsequently either dissociate or remain intact, migrate on the surface, penetrate into pores or diffuse into the bulk of the catalyst. The adsorbed species may react with either other compounds on the surface or gas-phase reactants. They can also desorb from the surface into the gas phase. A possible beneficial outcome of adsorption is increased reaction time and improved yield of products because of surface reactions. Compared to conventional

catalysis, combining catalysts with plasma provides additional reaction pathways that have lower energy barriers and higher rates [13].

The role of atomic oxygen and ozone is important in catalyst activation by plasma, as some catalysts have the ability to decompose ozone on the surface. In this process, a reservoir of O-radicals is created on the surface, which can in turn increase oxidation rates. Decomposition of ozone is also useful for reducing the amount of it escaping to the outlet of the system [13].

The effect of photocatalysis is based on the formation of electron-hole pairs as a consequence of plasma-generated UV-radiation, resulting in additional surface reactions. However, the importance if this effect is found to be smaller than those described previously [35, 36].

In addition to plasma modifying the catalyst surface, the presence of catalyst may also alter the properties of the discharge. For example, the addition of a dielectric material into a DBD reactor changes its capacitance. Surface roughness and the presence of pores can introduce local variations in the electric field, which can change the yield of chemical species in the discharge through altering the electron energy distribution [13]. A catalyst can also change the nature of the discharge, e.g. transitioning from volume to surface discharge, observed in case of $BaTiO_3$ and TiO_2 [37, 38].

In view of the above, a synergistic effect occurs, in which case the overall effect of plasma and catalyst combined is greater than the sum of the individual effects by plasma and catalyst separately. This can manifest in improved yields, selectivities of energy efficiency, etc. [13]

The interaction between plasma and catalyst is less complicated in the two-stage system. The main influence of plasma on the functioning of the catalyst is due to plasma-generated chemical species that have long enough lifetimes, so that they are able to travel from the discharge region to the surface of the catalyst. Typically those include, e.g. in case of air plasmas, ozone, NO and NO_2. Upon reaching the catalyst, these species can undergo adsorption and other surface processes. For example, decomposition of ozone has been found to be an important step in two-stage plasma-catalytic destruction of volatile organic compounds [39, 40]. Furthermore, chemical processes in the plasma may release energy that increases gas temperature, altering the working conditions of the catalyst. In addition, vibrationally exited molecules are created in plasma, which, depending on the rate of vibrational relaxation, may reach the catalyst surface [13].

2.5. Mathematical models of removal processes

Removal by NTP or plasma-catalytic systems has been extensively studied in case of volatile organic compounds (VOC). In direct plasma oxidation, O and OH radicals are the main reagents taken into account in global kinetic models [41, 42]. The radical production efficiency is usually assumed to be uniform within the discharge area and independent of input power and gas flow rate. The

radicals take part in oxidation reactions with the pollutants, as well as scavenging reactions, where they are lost to processes with other species. These processes can be described by the following general model [43]:

reaction	rate expression	
e + A → R + A’	$\frac{\mathrm{d}[\mathrm{R}]}{\mathrm{d}t} = GP$	(1)
R + X → products	$\frac{\mathrm{d}[\mathrm{X}]}{\mathrm{d}t} = -k[\mathrm{R}][\mathrm{X}]$	(2)
R + S_i → products	$\frac{\mathrm{d}[\mathrm{R}]}{\mathrm{d}t} = -\sum_i k_{\mathrm{S}i}[\mathrm{R}][\mathrm{S}_i]$	(3)

In these equations, X represents the pollutant, A is the carrier gas species, R is the radical and the symbols S_i represent scavenger species. The quantity G is the radical production efficiency, P is the plasma power density, k is the rate coefficient for the radical-pollutant reaction and k_{Si} is the rate coefficient for the i-th scavenging reaction.

The system of equations (1)–(3) can be solved numerically to obtain theoretical removal plots. Alternatively, although the decomposition processes of VOCs can be complicated, simplifications and approximations may be possible to obtain analytical expressions to characterize pollutant removal. For example, since reaction (2) is usually fast, it can be assumed that radicals R are consumed as quickly as they are created. In this case, steady-state approximation holds, i.e. the net rate of change of radicals $\mathrm{d}[\mathrm{R}]/\mathrm{d}t = 0$. This condition leads to an expression for the steady-state value of [R], the substitution of which into equation (2), followed by integration of the system yields an algebraic equation for [X]. At low degrees of removal this equation can be written in the simplified form

$$\frac{[\mathrm{X}]}{[\mathrm{X}]_0} = \exp\left(-\frac{E}{\beta}\right), \quad \beta = \frac{1}{G}\left([\mathrm{X}]_0 + \frac{\sum_i k_{\mathrm{S}i}[S_i]}{k}\right), \tag{4}$$

where E is the specific input energy (plasma power P divided by flow rate) and $[\mathrm{X}]_0$ is the initial concentration of the pollutant.

In conditions, where the rate of the useful oxidation reaction is much greater than the rate of radical scavenging, i.e. $k[\mathrm{X}]_0 \gg \sum k_{Si}[\mathrm{S}_i]$, the removal degree depends on $[\mathrm{X}]_0$, as shown by examples in Figure 1 (left). In the opposite case, where the scavenging reactions are faster, the initial concentration of the pollutant only weakly influences the removal degree (Figure 1, right) [43]. Usually the scavenging reactions are faster, which leads to a large fraction of

radicals being prevented from participating in pollutant oxidation reactions. As a consequence, the energy efficiency of the process is reduced. The necessary energy to reach a given oxidation degree could be reduced by introducing a catalyst, on the surface of which the radical pollutant reaction may be faster [44].

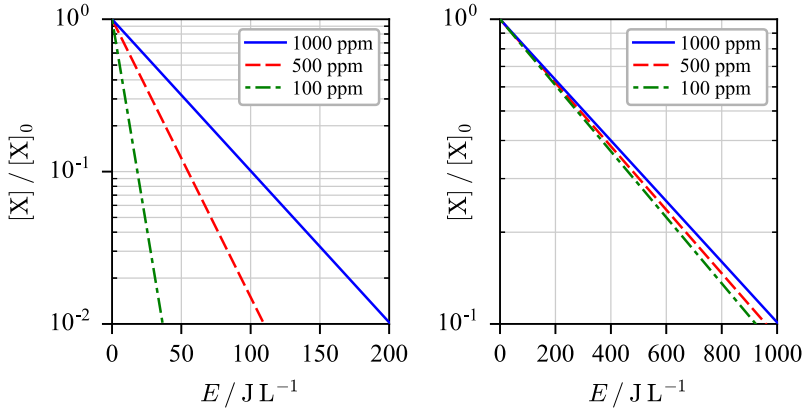

Figure 1. Examples of theoretical removal plots, comparing cases where the initial concentration of the pollutant is 100, 500 and 1000 ppm. On the left: radical attack dominates, on the right: scavenging reactions dominate.

Improvement due to catalysts is mainly connected with O and O_3, created in the plasma. As oxidation of VOC by ozone proceeds slowly [45], the formation of O_3 is considered a scavenging reaction, reducing the amount of necessary O-radicals. Decomposition of ozone on the surface of the catalyst can restore the supply of atomic oxygen and increase the overall efficiency of pollutant removal [46].

Similar principles may be considered in constructing mathematical models for NO_x removal and the addition of catalysts have led to improvements in the oxidation of NO [47, 48]. However, there are important differences between the oxidation of VOCs and NO_x, that need to be taken into account. As the reaction between NO and O_3 is fast, the conversion of O-radicals to O_3 is a useful reaction instead of a scavenging one [49]. On the other hand, in case of NO_x a back-reaction occurs, in which NO_2 reacts with O-radicals and NO is recreated [49, 50]. These differences influence the use of catalysts in the oxidation of NO in plasma-catalytic systems.

3. RESEARCH OBJECTIVES

The general goal in the studies included in the current thesis was to investigate the role of catalysts in the oxidation of NO_x by plasma species. The following division into subgoals was made.

The first objective was to compare the oxidation efficiency and the influence of catalysts in different experimental configurations. Experiments with direct oxidation of NO_x by plasma were carried out in a single-stage system; indirect plasma oxidation of NO_x was investigated, using a two-stage configuration for catalyst placement.

The second objective was to compare different materials that can be used as catalysts. For this, metal oxides TiO_2, γ-Al_2O_3 and γ-Fe_2O_3 were chosen, partly on the basis of their relatively low cost and easy availability, making them suitable for possible applications. Regarding applications, determining optimal conditions for the method was also part of the research agenda.

The final objective was to investigate processes taking place on the surface of catalysts. Within this aim, the following stages were carried out:

- calculating amounts of substances on the surfaces of different metal oxides at different conditions;
- identifying compounds on the surface by *in-situ* DRIFTS methodology;
- based on findings, proposing possible reaction mechanisms.

4. EXPERIMENTAL SETUP

4.1. General description

The experiments were conducted in a flow-through system, presented in Figure 2, which depicts the initial gas supply, different configurations of the plasma-catalytic system, and the measurement setup for gas phase reaction products.

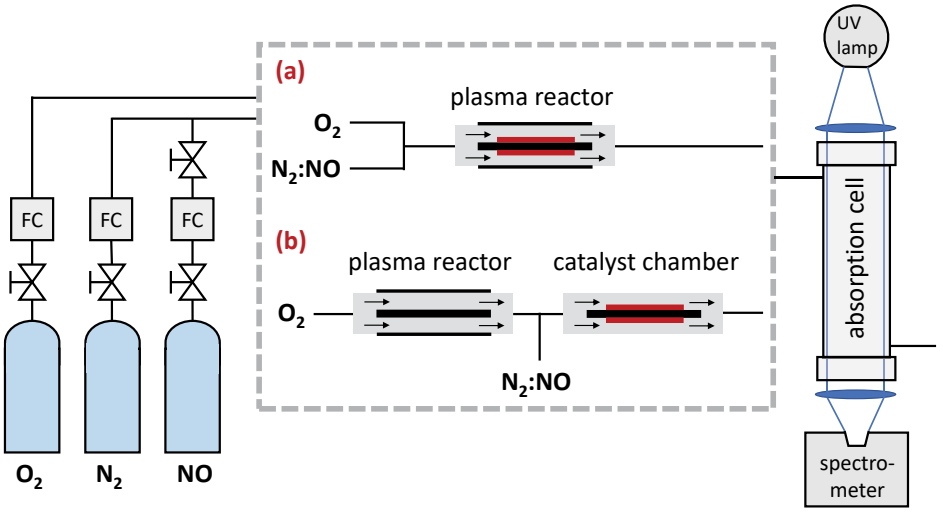

Figure 2. Experimental setup for direct oxidation by plasma (a) and indirect plasma oxidation (b).

The experiments were carried out in dry air conditions. The initial gas supply was composed of oxygen, nitrogen and NO, the flow rates of which were set with Alicat Scientific flow controllers. The total flow rate was 0.5–2 L/min. The oxygen content ranged from 10% to 50% in different experiments and the initial concentration of NO was 200–800 ppm.

The plasma-catalytic system was used in different arrangements, depending on the method of plasma usage. In case of direct oxidation by plasma, the mixture of N_2, O_2 and NO was directed through the plasma reactor, which also contained the catalyst powder. In case of indirect plasma oxidation, only the O_2 stream was directed through the plasma reactor, which was applied as an ozone generator. The resulting mixture of N_2, O_2, NO and O_3 was then directed through the catalyst chamber of the same build and dimensions. The plasma reactor and the catalysts are described in more detail in sections 4.2 and 4.3.

An electrically heated oven was used to set the temperature of the chamber containing the catalyst – either the plasma reactor in case of the single-stage arrangement or the catalyst chamber in case of the two-stage arrangement. The temperature was measured using an Osensa Innovations fiber-optical temperature sensor FTX-100-Gen.

The gas phase reaction products were detected by UV absorption and processes on the surface of the catalysts were monitored by DRIFTS. These methods are described in sections 4.4 and 4.5.

4.2. Plasma reactor

The DBD reactor (Figure 3) was of coaxial structure, with a stainless steel cylinder of 14 mm in outer diameter as the inner electrode. A quartz tube of 16.3 mm in inner diameter functioned as the dielectric barrier and a steel mesh around the tube functioned as the grounded electrode. The length of the reactor was 8.5 cm and, given the discharge gap of 1.15 mm, the volume of the active zone of the reactor was 4.7 cm^3. In the two-stage system, used for indirect plasma oxidation of NO_x, a second chamber with the same geometrical parameters was used for the placement of the catalyst.

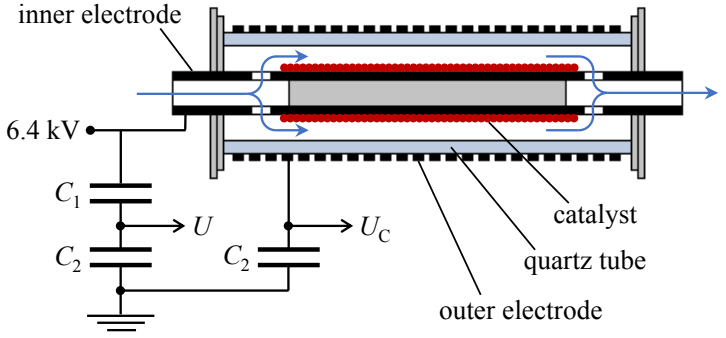

Figure 3. Longitudinal section schematic and circuit diagram of the plasma reactor in one-stage configuration, used for direct oxidation by plasma. Parameter values: $C_1 = 23$ pF, $C_2 = 21.3$ nF.

A sinusoidal voltage was generated by a signal generator HQ Power DVM20FGCN, which was connected to a power amplifier Industrial Test Equipment Co, Inc "Powertron" A 500 RF. The inner electrode of the plasma reactor was powered over a transformer with a turns ratio 1000. A capacitive voltage divider was used to measure the applied voltage and an additional capacitor was connected in series with the plasma reactor, to measure the charge accumulating on the dielectric surface (Figure 3). The voltage waveforms (U, U_C) were recorded by a digital oscilloscope Velleman PCS500. The range of frequencies used in the experiments was 100–5000 Hz and the peak-to-peak value of applied voltage was 14 kV.

The input power was measured by the method of Lissajous figures [34]. The plot of Q=C_2U_C vs U results in the appearance of a parallelogram, (Figure 4) the area of which is equal to the work done by the electric field during one period to displace charges. Multiplying this work by the frequency of the applied voltage

gives as a result the power directed into the discharge. The specific input energy (*SIE*) was obtained by dividing the input power with the gas flow rate through the plasma reactor.

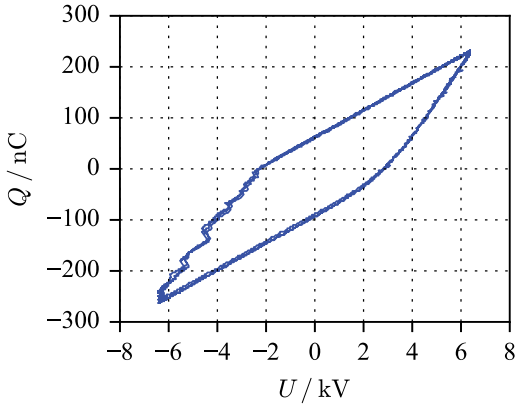

Figure 4. An example of a Lissajous figure, formed during the operation of the plasma reactor.

In experiments that were conducted with indirect plasma oxidation, an important quantity was the concentration of ozone at the inlet of the catalyst chamber. For this purpose, a separate series of calibration measurements without catalyst was carried out to obtain a relationship between *SIE* and the corresponding concentration of ozone, measured by UV absorption (section 4.4). The above-described setup enabled to control the value of *SIE* and, in case of indirect plasma oxidation, the concentration of ozone at the inlet of the catalyst chamber. Stemming from the uncertainty of *SIE*, the uncertainty of the inlet concentration of ozone was estimated to be within 10%.

4.3. Catalysts

Nanopowders of TiO_2, γ-Al_2O_3 and γ-Fe_2O_3 (Figure 5) were investigated for their effectiveness as catalysts. The powder was pressed on the inner wall of either the plasma reactor (in case of one-stage system) or the catalyst chamber (in case of one-stage system), forming a thin coating of 0.1–0.2 mm in thickness.

Figure 5. Metal oxide powders (from the left): TiO_2, γ-Fe_2O_3, γ-Al_2O_3.

Commercial Degussa P25 powder with 80% in anatase and 20% in rutile was used for the investigation of TiO_2. The diameter of the particles is below 25 nm and the specific surface area is above 50 m^2/g. The total mass of TiO_2 powder ranged from 0.3 g to 0.81 g in different studies included in the current thesis.

The powders of γ-Al_2O_3 and γ-Fe_2O_3 were obtained from Sigma Aldrich. Both powders consisted of particles below 50 nm in diameter and above 50 m^2/g in specific surface area. The total mass of γ-Al_2O_3 was 0.57 g and the total mass of γ-Fe_2O_3 ranged from 0.4 to 0.61 g in different studies.

One of the main reasons for selecting these materials as catalysts was their relatively low cost, especially compared to SCR catalysts, which contain precious metal additives. In addition, TiO_2 is known for its photocatalytic property [35], which provides a point of comparison with Al_2O_3 that has a large band gap. Fe_2O_3 is known for its activity in ozone degradation [51].

4.4. Detection of gas phase reaction products

To analyze the gas composition exiting the plasma-catalytic system, the mixture was directed through an optical absorption cell with the length of 20 cm. The absorption cell was illuminated by a Hamamatsu L7296-50 deuterium lamp and an Ocean Optics 4000 spectrometer was used to record the absorption spectra (Figure 2). The spectrometer has a 200–850 nm wavelength range and a 1.5–2.3 nm optical resolution.

Calculation of the concentrations of different gases was based on the Beer-Lambert law

$$I = I_0 e^{-\sigma N d},$$

where I_0 and I are the intensity of UV-radiation before and after the absorption cell, respectively, σ is the absorption cross-section of a specific gas molecule, N is the average concentration of these molecules in the absorption cell and d is the length of the absorption cell. The quantity given by the spectrometer is $A = \log(I_0/I)$, so the concentration of the substance is given by

$$N = \frac{2.303A}{\sigma d}.$$

The method enabled the measurement of concentrations of NO_2, N_2O_5 and O_3, with their absorption cross-sections obtained from MPI-Mainz UV/VIS spectral atlas [52]. To determine the concentration of NO, a separate calibration procedure was carried out with NO/N_2 mixtures of known compositions and without plasma generation.

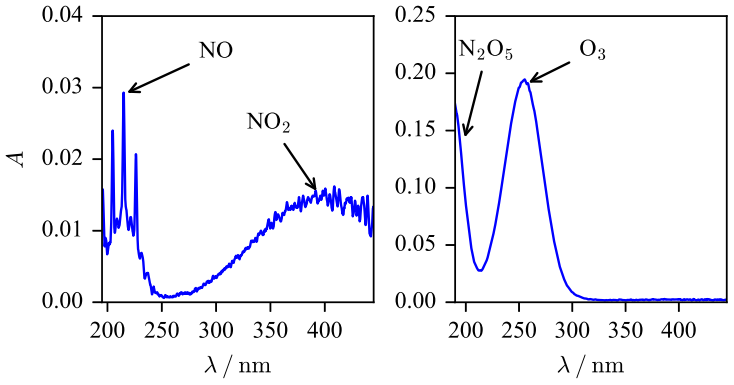

Figure 6. Examples of absorption spectra.

Figure 6 shows two examples of typical absorption spectra, corresponding to different gas compositions. The spectrum on left-hand panel was obtained with indirect plasma oxidation at low O_3 concentrations, with partial oxidation of NO to NO_2 and consequently no absorption bands visible for O_3 or N_2O_5. The spectrum on right-hand panel was obtained at high O_3 concentrations, in which case all of the NO_2 was oxidized to N_2O_5.

It can be seen that overlapping of different absorption bands is present, requiring additional data analysis procedures to subtract the absorption caused by different substances. This is especially the case for N_2O_5, for which obtaining the absorption around 200 nm band required the subtraction of absorption by both NO_2 and O_3. A separate experiment was carried out, in which case 1% of H_2O was added to the mixture, to verify that the absorption around 200 nm was not due to HNO_3 in the main experiments. The assignment of the absorption band to N_2O_5 was additionally confirmed by the fact that the sum of concentrations of NO, NO_2 and twice that of N_2O_5 corresponded to the inlet concentration of NO.

The considerations described above increased the uncertainty of the outlet concentrations. The uncertainty was additionally increased by adsorption of N_2O_5 on the windows of the absorption cell and the decrease of the sensitivity of the spectrometer below 200 nm. As a result, the estimated uncertainty for the outlet concentration was 15 ppm for NO, 20 ppm for NO_2 and 30 ppm for N_2O_5.

4.5. Detection of surface species by DRIFTS

In case of TiO_2 with indirect plasma oxidation, additional series of experiments were carried out with a modified setup to study the catalyst surface directly. For that purpose, diffuse infrared Fourier transform spectroscopy (DRIFTS) was applied.

Instead of using the catalyst chamber similar to the plasma reactor, 30 mg of TiO_2 powder was placed in a smaller chamber with a powder sample holder and

a ZnSe window. The IR spectra were recorded using an Interspec 2020 spectrometer supplied with a Pike Technologies DiffusIR diffuse reflectance accessory. The spectral resolution of the spectrometer was 4 cm^{-1}, 5–100 scans were accumulated for one spectrum. The catalyst chamber was heated to 100 °C by an electrical heating tape. The spectra were recorded with various inlet concentrations of NO and O_3, which were similar to other experiments, and the reference spectra were obtained with NO as the only nitrogen oxides species in the gas stream.

5. RESULTS AND DISCUSSION

5.1. Direct oxidation of NO_x by plasma

In direct oxidation by plasma the gas mixture consisting of N_2, O_2 and NO was directed to the inlet of the plasma reactor, which was turned on for 5 minutes. The concentrations of gas-phase reaction products were measured at the outlet by UV absorption. The results that are presented in the current section, were obtained in experiments, where the total flow rate was 1 L/min, the O_2 content in the initial mixture was 10% and the inlet concentration of NO was 360 ppm. The temperature in the plasma reactor was 110 °C and the catalytic effect of Fe_2O_3 was investigated [**I**].

Figure 7 presents the outlet concentrations of NO and NO_2 at different values of specific input energy (*SIE*), measured in experiments without catalyst. The oxidation of NO to NO_2 can be seen, with the conversion degree increasing with *SIE* at values below 100 J/L. At higher values of *SIE*, starting from approximately 100 J/L, a saturation effect occurs, in which the concentrations of NO and NO_2 remain constant while increasing *SIE*. This effect indicates a significant limitation on the effectiveness and applicability of the oxidation of NO directly by plasma. Both the saturation values and the oxidation efficiencies at low *SIE* values (characterized by the slope of the tangent line of the NO_2 curve of Figure 7) depended on the O_2 fraction and temperature and exhibited tendencies similar to those obtained with a surface barrier discharge reactor [53].

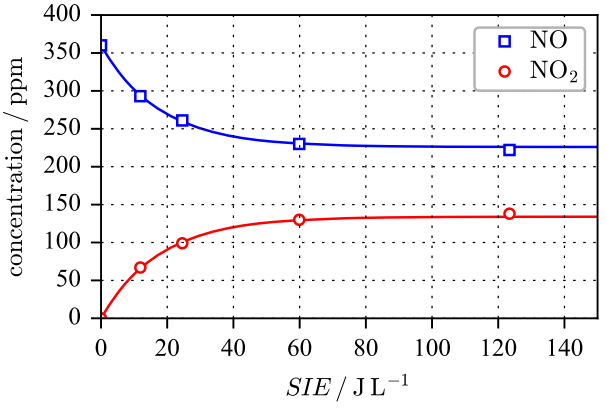

Figure 7. The outlet concentrations of NO and NO_2, as functions of specific input energy (*SIE*), in direct oxidation by plasma without catalyst. The inlet concentration of NO was 360 ppm, temperature 110 °C. The theoretical curves are calculated by Eq. (9).

The results shown in Figure 7 can be numerically simulated, using the following reactions and corresponding rate coefficients:

$$O + O_2 + M \rightarrow O_3 + M, \qquad k_1 = 5.6\times10^{-34}(T/298)^{-2.6}\ \mathrm{cm^6\ s^{-1}}, \tag{5}$$

$$O + NO + M \rightarrow NO_2 + M, \qquad k_2 = 8.6\times10^{-32}(T/298)^{-1.8}\ \mathrm{cm^6\ s^{-1}}, \tag{6}$$

$$O + NO_2 \rightarrow NO + O_2, \qquad k_3 = 5.5\times10^{-12}\ e^{1.56/RT}\ \mathrm{cm^3\ s^{-1}}, \tag{7}$$

$$NO + O_3 \rightarrow NO_2 + O_2, \qquad k_4 = 2\times10^{-12}\ e^{-11.64/RT}\ \mathrm{cm^3\ s^{-1}}. \tag{8}$$

where T is the temperature in K inside the plasma reactor and $R = 8.31\,\frac{\mathrm{J}}{\mathrm{mol\times K}}$ is the universal gas constant. The expressions and parameters for the rate coefficients were obtained from the NIST Chemical Kinetics Database [54].

The main oxidizing agent is the atomic oxygen radical, which is responsible for both the oxidation of NO to NO_2 and ozone production [7] [**I**]. Ozone is mostly consumed in reaction with NO (8), while part of it leaves the reactor. Reaction (7) provides an explanation for the limit on NO removal degree, which is the reaction of the O-radical with NO_2 to reproduce NO. At *SIE* values corresponding to saturation of NO and NO_2 concentrations, the oxidation of NO and the back-reaction reach equilibrium, which is shifted towards the back-reaction, when temperature is increased.

Based on scientific literature, it should be added, that the oxidation efficiency of NO to NO_2 has been found to be significantly increased in the presence of hydrocarbons. In that case the back-reaction of NO_2 to NO would be suppressed by the consumption of O radicals in hydrocarbon degradation reactions. This chain of reactions would result in the formation HO_2 radicals and hydrocarbon fragments that would in turn contribute to further oxidation of NO [55].

Addition of the Fe_2O_3 powder into the plasma reactor resulted in increased conversion of NO to NO_2. The resulting increase of NO_2 concentration is shown in Figure 8. The effect of the catalyst starts to become significant at *SIE* values above 50 J/L. The improvement is limited, reaching a 35% increase in NO_2 concentration at *SIE* values corresponding to saturated levels of NO and NO_2.

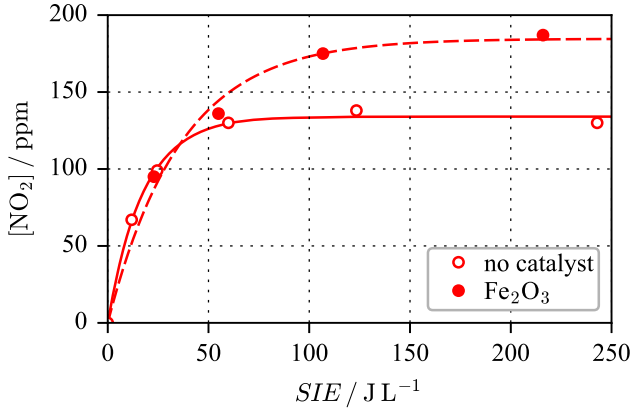

Figure 8. Comparison of outlet concentrations of NO_2, obtained with and without Fe_2O_3 in the plasma reactor. The inlet concentration of NO was 360 ppm, temperature 110 °C. The theoretical curves are calculated by Eq. (9).

Analysis of reactions (5)–(8), along with approximations described in our paper [**IV**] and a previous publication [49], allows the derivation of an analytical function to describe the dependence of the NO_2 outlet concentration on *SIE*:

$$[\mathrm{NO_2}] = \Delta[\mathrm{NO}]_{\max}\left[1 - \exp\left(-\frac{SIE}{\beta}\right)\right], \tag{9}$$

where

$$\Delta[\mathrm{NO}]_{\max} = \frac{k_2[\mathrm{NO}]_0 + k_1[\mathrm{O_2}] + r_c}{k_2 + \frac{k_3}{n}}, \tag{10}$$

$$\beta = \frac{k_3(k_2[\mathrm{NO}]_0 + k_1[\mathrm{O_2}] + r_c)}{1.3 G_O n \left(k_2 + \frac{k_3}{n}\right)^2}. \tag{11}$$

$[NO]_0$ is the inlet concentration of NO, $\Delta[NO]_{max}$ is the maximum reduction of the concentration of NO and n is the gas number density. The influence of catalyst is described by the additional term r_C, which represents the rate of oxidation on the surface.

G_O is the oxygen radical production efficiency, defined as the number of O-radicals created in plasma per unit value of *SIE*. It is assumed that the production of O-radicals takes place uniformly within the discharge region, characterized by an average value of G_O. The value of G_O has been estimated in separate experiments of ozone production, which at low *SIE* values takes place

according to the expression $[O_3] = G_O \times SIE$. As an example, in our reactor G_O = 12 ppm/(J L^{-1}) in air [53].

According to Eq. (10), the maximum amount of oxidized NO increases with $[NO]_0$ and the O_2 fraction and decreases with temperature. It is, however, independent of G_O, the increase of which could only improve the oxidation al low *SIE* values, where $\Delta[NO]_{max}$ is not reached. Similar results were obtained is parallel with TiO_2 as catalyst material [47, 56].

The previous discussion was focused on the analysis of stabilized outlet concentrations at different *SIE* values. The stabilization times increased considerably, when Fe_2O_3 was used, compared to oxidation without catalyst. This effect was observed by collecting time series data, for which a new absorption spectrum was recorded every 5–6 seconds. An example, showing the time dependence of the outlet concentrations of NO and NO_2, is presented in Figure 6 in publication [**I**].

It was observed that the concentrations of NO and NO_2 take at least a minute to reach their stationary values both at the beginning of plasma treatment and after the end of it. Furthermore, an important phenomenon is revealed in the time dependence of the sum of the two concentrations. Following the switch-on of the plasma reactor, the total concentration decreases to a minimum and returns to approximately its original value in a few minutes. The reverse effect takes place after the switch-off of the plasma reactor, which brings about a temporary surplus of NO_x, compared to the inlet concentration of NO. We attribute these effects to the adsorption and desorption of NO_x on the surface of the catalyst. This interpretation is reinforced by analysis of equivalent effects in oxidation by ozone, discussed in section 5.3, where they are connected to the formation of a specific surface compounds.

5.2. Oxidation of NO_x by ozone

5.2.1. Time-dependent outlet concentrations

In case of indirect plasma oxidation, the plasma reactor functioned as an ozone generator and the catalysts were placed in a different chamber downstream of the plasma reactor. The catalysts, the effects of which were investigated, are TiO_2, Al_2O_3 and Fe_2O_3. For comparison, oxidation of NO_x by ozone without catalysts was also studied. For each catalyst, as well as the absence of catalyst, an extensive parameter space was explored.

When plasma is used indirectly, ozone is the only oxidizing agent created in the discharge with a long enough lifetime to exit the plasma reactor. Therefore, instead of *SIE*, the inlet concentration of ozone $[O_3]_0$ was used to characterize the operation of the plasma reactor. This quantity was changed in the range 200–1500 ppm. The values 200, 400 and 800 ppm were used for the inlet concentration of NO. The experiments were carried out at catalyst chamber temperatures 20–140 °C. In publications [**II**] and [**III**] the influence of changing

the total flow rate was also investigated, comparing the values 0.5, 1 and 2 L/min. In all of the experiments with the two-stage system, the oxygen content in the initial gas mixture was 50%.

For each specific combination of these parameters, time series data was recorded for the outlet concentrations of NO, NO_2, N_2O_5 and O_3 by storing a new absorbance spectrum every 5–6 seconds. Figure 9 presents a few characteristic examples of the results of these individual experimental cycles, comparing different regimes of NO_x oxidation and demonstrating the typical effects of adding a catalyst. In these examples TiO_2 was used as the catalyst, the inlet concentration of NO was 800 ppm, the total flow rate was 1 L/min and the catalyst chamber was heated to 100 °C. There are several general aspects to note on the basis of these time dependencies.

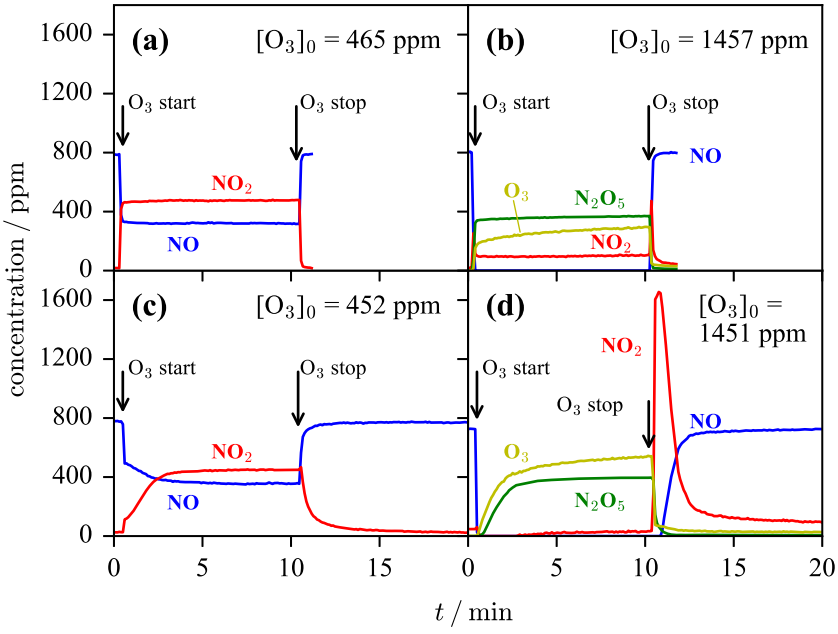

Figure 9. Characteristic examples of time-dependent outlet concentrations: a, c – only NO and NO_2 were present in the outlet mixture during O_3 production; b, d – NO was completely oxidized and N_2O_5 was formed; a, b – no catalyst; c, d – TiO_2 used as catalyst. $[NO]_0$ = 800 ppm, T = 100 °C, total flow rate 1 L/min.

The first aspect to note is the influence of the inlet concentration of ozone, which is the main factor that influences the steady-state concentrations during NO_x oxidation and which determines the oxidation regime. In the NO_2 production regime (panels a, c) the inlet concentration of NO is greater than the inlet concentration of O_3. As a result, a fraction of the NO content is quickly converted to NO_2, consuming all of the O_3 being produced. The steady-state values of concentrations remain unchanged after adding the catalyst and N_2O_5 does not appear in the outlet.

In the N_2O_5 production regime (panels b, d) the initial concentration of O_3 is greater than that of NO. As a result, all of the NO is oxidized to NO_2, leaving a fraction of the initial O_3 content available to participate in the slower reaction of NO_2 being oxidized to N_2O_5. The steady-state concentrations show the disappearance of NO and the appearance of both N_2O_5 and O_3 in the outlet. A reduced amount or total disappearance of NO_2 is also observed during the oxidation period.

Another set of characteristic features visible from the time-dependencies has to do with the rates of change in the outlet concentrations immediately after both the beginning and the end of O_3 production. In case of oxidation by ozone without catalyst (panels a, b) the outlet concentrations on NO, NO_2 and N_2O_5 quickly settle on their steady-state values during O_3 production and immediately resume their original levels after the end of O_3 production.

A very different picture emerges when a catalyst is present (panels c, d). In both the NO_2 and the N_2O_5 regime the outlet concentrations take several minutes to stabilize after the start of O_3 production. Additional transient processes can be seen at the end of O_3 production in the N_2O_5 regime (panel d), most notably a spike in NO_2 before its disappearance from the outlet. It can also be seen that NO reappears in the outlet only after the concentration of NO_2 starts to decline and N_2O_5 has disappeared. In our publications included in the current thesis, we have attributed these transient changes in the presence of a catalyst to processes connected with adsorption and desorption of various compounds on the surface.

For each of the studied metal oxides, the first measurement cycle after the placement of new powder into the catalyst chamber produced different results, compared to the second at the same conditions, mainly with longer stabilization times. Subsequent cycles, however, yielded repeatable results. All of the measurements presented in the current thesis were preceded by an initial session of catalyst pretreatment and the following data analysis is based on repeatable results.

In the current section we continue with the analysis of steady-state concentrations to investigate the overall efficiency of NO_x oxidation by ozone and metal oxides. Section 5.3 deals with the analysis of time-dependent changes to investigate processes on the catalyst surface.

5.2.2. Characterization of oxidation efficiency

With fixed values for temperature, inlet concentration of NO and flow rate, a series of measurement cycles were conducted at various inlet concentrations of O_3. Figure 10 presents the results of a typical example of such experimental series, plotting the steady-state values of the outlet concentrations of nitrogen oxides, reached during the oxidation phase, against the concentration of ozone produced by the plasma reactor. In this case the inlet concentration of NO was 400 ppm, the temperature of the catalyst chamber was 60 °C and the total flow rate was 1 L/min. The results shown were obtained without catalyst.

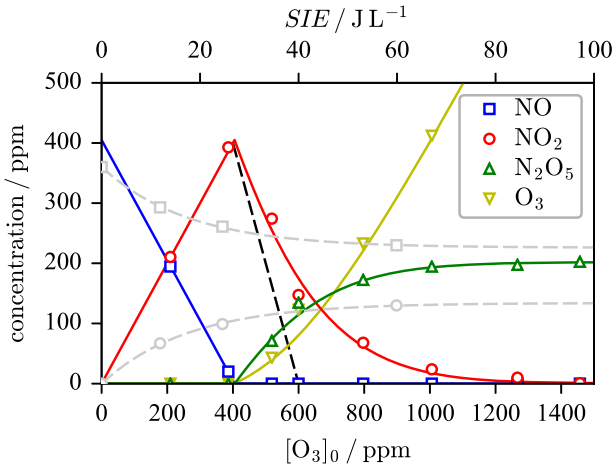

Figure 10. Steady-state outlet concentrations of NO, NO_2, N_2O_5 and O_3 in case of oxidation by ozone as functions of the inlet concentration of ozone, $[O_3]_0$. The results are obtained without catalyst at $[NO]_0$ = 400 ppm, T = 60 °C, flow rate 1 L/min. The concentrations of NO and NO_2 in the single-stage system, shown in light gray color, are reproduced from Figure 7 for comparison.

At $[O_3]_0 < [NO]_0$ the decrease of NO and the increase of NO_2 followed linear functions, given by the relations $[NO_2] = [O_3]_0$ and $[NO] = [NO]_0 - [O_3]_0$. At $[O_3]_0 > [NO]_0$ the concentration of NO_2 decreases with the increase of $[O_3]_0$ and N_2O_5 appears in the outlet. At high enough values of $[O_3]_0$, practically all of NO_2 was removed. In addition, unreacted ozone was visible in the outlet at high values of $[O_3]_0$.

It should be noted that oxidation of NO_x proved much more efficient, compared to direct oxidation by plasma, as seen from the comparison shown in Figure 10. The value $[O_3]_0$ = 400 ppm, which corresponds to complete removal of NO in case of oxidation by ozone, was achieved at $SIE \approx 27$ J/L. At that value, only about 30% of NO was removed in case of direct oxidation by plasma [**IV**]. The most important factor causing this difference is the absence of the back-reaction (7), which is due to the fact that unlike direct plasma oxidation, NO_2 is not exposed to reactions with atomic oxygen in case of oxidation only by ozone.

Without catalyst, the tendencies described above are explained by the following gas-phase reactions, given with their corresponding rate coefficients [57]:

$$\mathrm{NO} + \mathrm{O_3} \rightarrow \mathrm{NO_2} + \mathrm{O_2},$$
$$k_4 = 2 \times 10^{-12} \exp\left(-\frac{11.64}{RT}\right) \frac{\mathrm{cm}^3}{\mathrm{s}}, \tag{12}$$

$$\mathrm{NO_2} + \mathrm{O_3} \rightarrow \mathrm{NO_3} + \mathrm{O_2},$$
$$k_5 = 1.2 \times 10^{-13} \exp\left(-\frac{20.37}{RT}\right) \frac{\mathrm{cm}^3}{\mathrm{s}}, \tag{13}$$

$$\mathrm{NO_2 + NO_3 + M \rightarrow N_2O_5 + M},$$
$$k_6 = 2.8 \times 10^{-30} \left(\frac{T}{298}\right)^{-3.5} \frac{\mathrm{cm^6}}{\mathrm{s}}, \tag{14}$$

$$\mathrm{N_2O_5 + M \rightarrow NO_2 + NO_3 + M},$$
$$k_7 = 10^{-3} \left(\frac{T}{298}\right)^{-3.5} \exp\left(-\frac{91.46}{RT}\right) \frac{\mathrm{cm^6}}{\mathrm{s}}, \tag{15}$$

where T is the temperature in K and $R = 8.31 \frac{\mathrm{J}}{\mathrm{mol \times K}}$ is the universal gas constant. Since $k_4 \gg k_5$, this model accounts for the lack of N_2O_5 in the NO_2 production regime ($[O_3]_0 < [NO]_0$).

Rate coefficients for the reactions (12)–(15) allow for numerical modelling of the oxidation of NO_x by ozone. In addition, based on quantitative analysis of rate coefficients presented in our publications [**II**, **IV**], the process of NO_2 oxidation to N_2O_5 can be modelled by the analytical function

$$\frac{[\mathrm{NO_2}]}{[\mathrm{NO}]_0} = \frac{2x - 3}{(2x - 2)\exp\{(2x - 3)[\mathrm{NO}]_0 k\tau\} - 1} \tag{16}$$

where $x = [O_3]_0/[NO]_0$ and $[NO]_0$ in Eq. (16) is the absolute concentration of NO at the inlet. The quantity τ is the total residence time, which in our experimental setup is calculated to be 2.9 s at total flow rate 1 L/min. The parameter k will be referred to as the effective rate coefficient. Eq. (16) is applied to calculate the solid curves on Figure 10, using the value $k = 4.47 \times 10^{-17}$ cm^3/s.

Without catalyst, the amount of ozone necessary to oxidize NO_2 to N_2O_5 was significantly greater than $1.5 \times [NO]_0$, which would follow from the stoichiometry of the overall process $2NO + 3O_3 \rightarrow N_2O_5 + 3O_2$ (Figure 10, black dashed line). The theoretical NO_2 removal function (16) is shifted towards the stoichiometric removal line by increasing the value of the effective rate coefficient k. Therefore, k can be used to quantify the efficiency of NO_2 oxidation, even though it describes the overall process in a volume that includes zones of different temperature. Analysis of function (16) shows that to achieve 95% removal of NO_2 at $x = 1.5$, the value of k would have to be increased to 7.4×10^{-16} cm^3/s at 60 °C and to 8.3×10^{-16} cm^3/s at 100 °C.

5.2.3. The effect of metal oxides on oxidation efficiency

Similar general tendencies as seen on Figure 10 were also observable at different temperatures and in the presence of metal oxide powders in the catalyst chamber. In order to compare the oxidation process in different series of experiments, it is sufficient to only compare the concentrations of NO_2, since its values are in direct correlation with those of NO and N_2O_5.

Figure 11 presents one such comparison to demonstrate the influence of different metal oxides in the catalyst chamber at 100 °C, with inlet concentration of NO at 400 ppm and flow rate 1 L/min. In the NO_2 production regime ($[O_3]_0/[NO]_0 < 1$) the metal oxide powders have no effect on the steady-state concentration of NO_2 and only influence the duration of transient processes, as explained in section 5.2.1. In the N_2O_5 production regime ($[O_3]_0/[NO]_0 < 1$) the influence of metal oxides as catalysts is clearly observed. Compared to the case of no catalyst, both TiO_2 and Al_2O_3 lead to an improvement of NO_2 oxidation, having the same effect within uncertainty. Fe_2O_3 results in the greatest improvement.

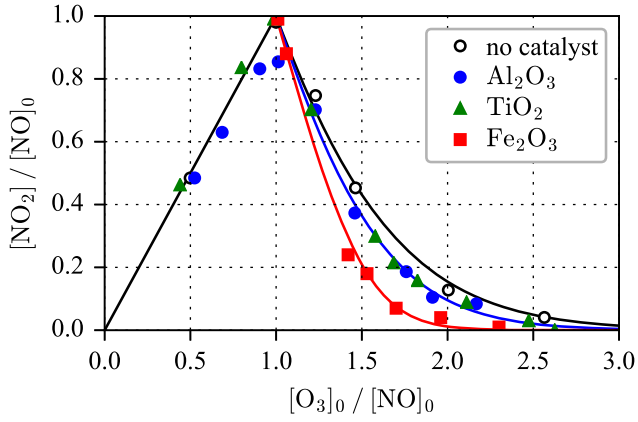

Figure 11. Normalized outlet concentrations of NO_2 as functions of the inlet concentration of O_3. $[NO]_0 = 400$ ppm, $T = 100$ °C, flow rate 1 L/min [**V**].

Formula (16) is used to calculate the theoretical curves on Figure 11. In terms of the values of the effective rate coefficient k, Fe_2O_3 results in an increase from 4.5×10^{-17} cm^3/s to 1.3×10^{-16} cm^3/s, whereas 95% removal at $x = 1.5$ at 100 °C would be reached in case of $k = 8.3\times10^{-16}$ cm^3/s (section 5.2.2). Although formula (16) is derived, based on only gas-phase reactions (12)–(15), the effective rate coefficient can still be used as a fitting parameter to quantify the influence of catalysts on the oxidation process.

Values of the effective rate coefficient were calculated at different temperatures and in case of different catalysts by fitting the NO_2 removal curves given by Eq. (16) to data points, obtained from the corresponding experimental series. The results are presented in Figure 12. There is no significant effect by the catalysts up to 60 °C. At 80 °C a noticeable effect is observed and at 100 °C the increase of k is at the maximum, achieved in case of Fe_2O_3. At 120 °C the value of k returns approximately to its value at 80 °C in case of Fe_2O_3 and to its value at 20 °C in case of no catalyst.

The decrease of the effective rate coefficient at temperature above 100 °C can be explained by the temperature dependence of the rate coefficient for gas-phase reaction (15), in which N_2O_5 decomposes and NO_2 is reproduced. While slower at low temperatures, the disintegration of N_2O_5 becomes more significant

as temperature is increased. At above 100 °C the rate of this reaction exceeds the overall rate of N_2O_5 production. The results suggest that the optimal temperature range for NO_x oxidation for the two-stage system is 80–120 °C.

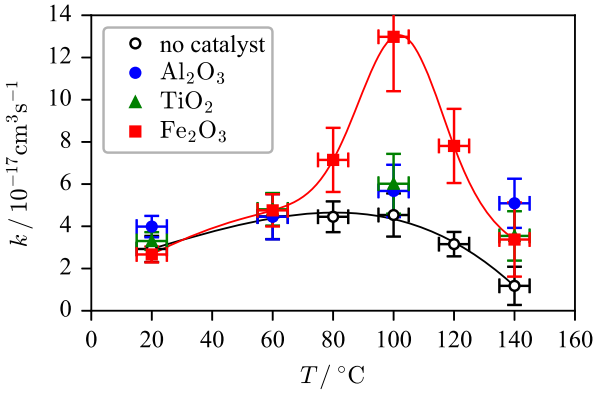

Figure 12. Dependence of the effective rate coefficient (k) on catalyst chamber temperature (T) for different metal oxides. The inlet concentration of NO was 400 ppm. The solid curves are added as a guide to the eye [**V**].

5.2.4. Decomposition of ozone by metal oxides

In addition to the catalytic effect of increasing the efficiency of NO_2 oxidation to N_2O_5, another important use of the metal oxide powders is the reduction of plasma-generated secondary ozone pollution in the outlet of the system.

To compare the ozone decomposing ability of different metal oxides, an additional series of measurements was carried out in the same two-stage configuration (case b in Figure 2) but without NO in the initial gas stream. The inlet concentration of ozone was kept at 350 ppm and the outlet concentration was measured during each measurement cycle that lasted for 10 minutes at a constant temperature. The measurement cycles were repeated at different temperatures and the results are presented in Figure 13 (left). The influence of Al_2O_3 becomes apparent at approximately 80 °C, while the decomposition of ozone starts at 60 °C in case of TiO_2. By far the most effective is Fe_2O_3, which destroys 40% of the inlet ozone already at room temperature and results in almost complete elimination of O_3 at 60 °C. From this point of view, as well as based on comparison of rate coefficient increase, Fe_2O_3 is shown to be the most suitable of the metal oxides studied in the current thesis [**V**].

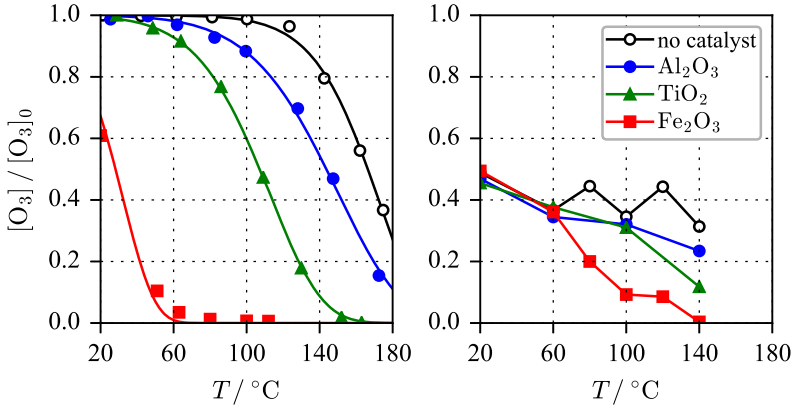

Figure 13. Dependence of the outlet concentration of ozone on the temperature (T) of the catalyst chamber in case of different metal oxides. On the left: results of ozone decomposition experiments without inlet NO. On the right: results from NO_x oxidation experiments, showing the amount of outlet ozone corresponding to 80% removal of NO_2.

For comparison, normalized outlet concentrations of O_3 in the NO_x oxidation experiments are presented in Figure 13 (right) at different temperatures. Linear interpolation was used to obtain the value of $[O_3]/[O_3]_0$ that corresponds to the state where 90% of the maximum amount of NO_2 has been oxidized to N_2O_5. The data is taken from experiments where $[NO]_0$ = 400 ppm, therefore the values of $[O_3]/[O_3]_0$ are presented in conditions where $[NO_2]$ = 40 ppm. Without metal oxides, the outlet concentrations of ozone at this NO_2 level were above 300 ppm at all temperatures. At 80 °C or higher, $[O_3]$ remained below 300 ppm in case of Al_2O_3 and TiO_2, and below 150 ppm in case of Fe_2O_3.

In case of no catalyst, Al_2O_3 and TiO_2, the outlet concentration of O_3 is reduced in the presence of NO in the initial gas composition, compared to O_3 decomposition without NO, because part of the ozone is consumed in the oxidation of NO_x. Fe_2O_3 results in a smaller amount of O_3 in the outlet, compared to other metal oxides. However, compared to the case without NO at the inlet, Fe_2O_3 leads to a higher concentration of O_3 in the outlet in the presence of NO, between 50 °C and 100 °C. This indicates that nitrogen oxides, created in oxidation of NO by ozone, reduce the ozone-decomposing ability of Fe_2O_3 [**I**]. A possible reason for this effect may be the blocking of surface sites by nitrogen oxides.

5.3. Investigation of surface processes

5.3.1. Indirect analysis of surface species

In order to gain information about the fundamental mechanism of the catalytic effect, processes on the surfaces of the metal oxides were investigated in case of oxidation of NO_x by ozone. For this purpose, time-dependent changes were

analyzed, such as those taking place at the beginning and shortly after the end of ozone production, described in subsection 5.2.1. The analysis presented in this section is largely based on publication [**III**].

The sum of nitrogen oxide concentrations is analyzed, defined as

$$[N_xO_y] = [NO] + [NO_2] + 2[N_2O_5]. \quad (17)$$

The concentration of N_2O_5 is multiplied by 2 for the purpose of obtaining the total number nitrogen atoms contained in the molecules of NO, NO_2 and N_2O_5. Provided that there are no processes that either remove or add nitrogen oxides from or to the gas phase, the quantity $[N_xO_y]$ should remain constant in time and equal to $[NO]_0$. This was confirmed by data from experiments without catalyst.

In experiments with a catalyst, however, $[N_xO_y]$ exhibited time-dependent changes, examples of which are shown in Figure 14 (upper panel). The start of ozone production was followed by a sharp drop of $[N_xO_y]$ and a subsequent return to the original value after several minutes. Both the initial decrease and time taken to resume the original value depended on the inlet concentration of ozone. Equivalent effects were evident after the end of ozone production, with a sharp increase, followed by a decrease, the size and duration of which increased with increasing inlet concentration of ozone. Both the increase of $[NO]_0$ and the increase of the total gas flow rate had the effect of reducing the time, during which $[N_xO_y]$ returned to its original value.

The deficit of nitrogen oxides in the gas phase at the beginning of ozone production indicates the process of adsorption on the metal oxide surface in that time period. Equivalently, desorption from the surface is indicated by the surplus of nitrogen oxides in the gas phase after the end of ozone production. Detailed analysis of time durations of the effects described above suggests that the inlet concentration of NO and flow rate have negligible influence on the total number of adsorbed surface species [**III**].

The interpretation above allows the quantification of adsorbed and desorbed species. The total number of nitrogen atoms within nitrogen oxides missing from or in surplus in the gas phase during one measurement cycle is proportional to the area of one of the shaded regions in Figure 14 (upper panel). Therefore, the amount of adsorbed substances can be obtained by integration of the function $[NO]_0 - [N_xO_y]$ with respect to time (or integration of $[N_xO_y] - [NO]_0$ for the amount of desorbed substances). Generalizing this principle allows us to write the following formula for the time-dependent adsorption function, which expresses the amount of substance per unit mass of catalyst, that is adsorbed by time t:

$$A(t) = \frac{F}{m}\int_0^t ([NO]_0 - [N_xO_y])\mathrm{d}t', \quad (18)$$

In this formula, F is the total gas flow rate and m is the mass of the catalyst. Function $A(t)$ is plotted in Figure 14 (lower panel).

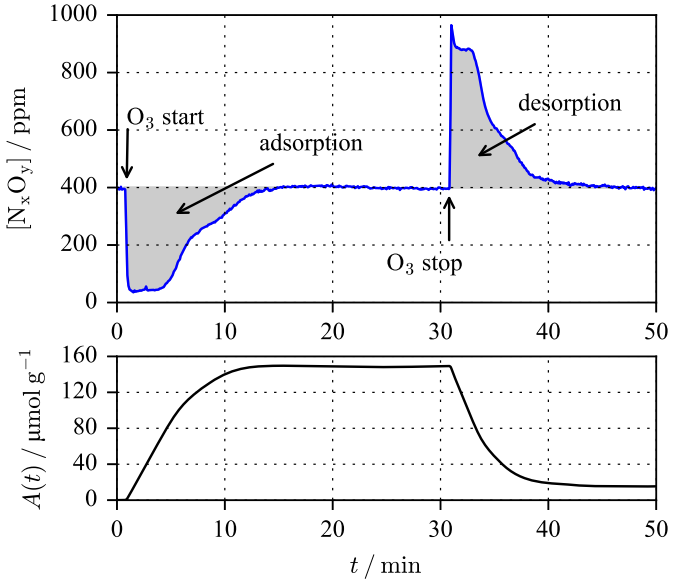

Figure 14. Correspondence between transient effects in the outlet concentration of gas-phase products and surface processes. Upper panel: sum of concentrations $[N_xO_y]$ as a function of time; adsorption and desorption are indicated by shaded regions. Lower panel: values of time-dependent adsorption, calculated by formula (18). TiO_2 was used as catalyst, T = 100 °C, $[O_3]_0$ = 674 ppm, flow rate 1 L/min.

Figure 15 presents the amounts of desorbed substances, i.e. the values of $N_{des} = A(t_1) - A(t_2)$, where t_1 is the moment of stopping ozone production and t_2 is the moment, when $[N_xO_y]$ has returned to the value $[NO]_0$. The values of N_{des} are given for different metal oxides and different values of the inlet concentration of ozone ($[O_3]_0$). At lower values of $[O_3]_0$ the dependence is approximately linear, but is followed by a sharp increase to at least 2 times higher value at the transition between the NO_2 and N_2O_5 production regimes. As $[O_3]_0$ is increased further, N_{des} stabilizes at 170–180 µmol/g in case of TiO_2 and Al_2O_3 and 120 µmol/g in case of Fe_2O_3. The values for TiO_2 and Al_2O_3 coincide within uncertainty. The amounts of substance on the surface of Fe_2O_3 were also lower in case of other temperatures [**V**].

Additional results with TiO_2 as catalyst, obtained at different values of inlet concentration of NO, indicate that in the NO_2 production regime the amount of substance on the surface depends on both the concentration of NO and NO_2 in the gas flow reaching the surface an is approximately inversely proportional to the concentration of NO [**III**].

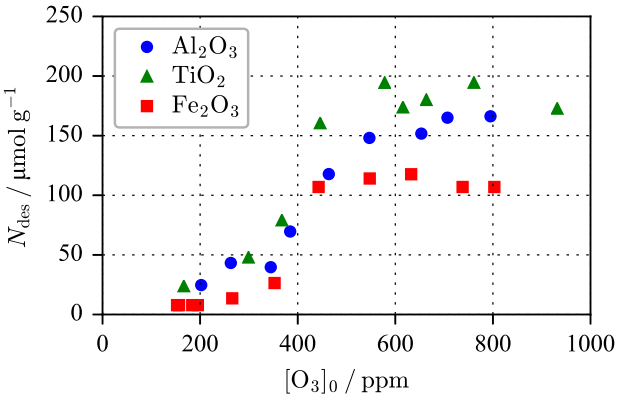

Figure 15. The amount of desorbed nitrogen oxides (N_{des}) from the surface, per unit mass of metal oxide. $[NO]_0$ = 400 ppm, T = 100 °C, flow rate 1 L/min [**V**].

5.3.2. Analysis of surface species by DRIFTS

DRIFTS measurements were carried out in two additional series of experiments with TiO_2, using a modified measurement setup, described in section 4.5. The aims of these experiments were to validate the interpretation of adsorption and desorption, as was stated in subsection 5.3.1, and to identify the composition of surface compounds. In all cases the gas flow rate was 1 L/min and the temperature of the catalyst chamber was 100 °C. In the first series of experiments 100 spectra were collected to be averaged after stable conditions were reached during ozone production. The collection of the spectra lasted for approximately 20 minutes, which prevented the observation of time-dependent changes, but provided detailed information about different absorption bands.

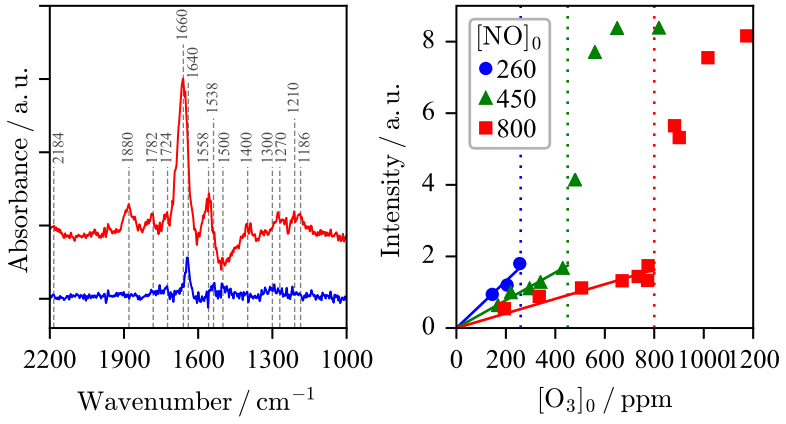

Figure 16. DRIFTS results with 100 scans to average. On the left: spectra obtained for the NO_2 and N_2O_5 regimes at $[NO]_0$ = 430 ppm. On the right: integrated intensity of the peak between 1600 and 1720 cm^{-1}, at different values of $[O_3]_0$ and $[NO]_0$. In the legend, the inlet concentrations of NO are expressed in ppm [**III**].

Figure 16 (left) presents two typical spectra: one obtained for the NO_2 and one for the N_2O_5 production regime. The most important peak at 1640 cm^{-1} and 1660 cm^{-1} is associated with bridging NO_3^- [19, 58–60]. Its intensities at different values of inlet concentration of O_3 are shown in Figure 16 (right), exhibiting similar trends to those visible in the behavior of the total amounts of adsorbed nitrogen oxides, determined by UV absorption of gas-phase products. In the NO_2 production regime, the intensity of the NO_3^- band increased with the increase of $[O_3]_0$ and therefore, with the increase of $[NO_2]$.

Transition to the N_2O_5 production regime was associated with a sharp increase to a much higher value, as well as a shift of the band towards higher wavenumbers. Other bands visible in the spectrum in the N_2O_5 production regime included those of bidentate NO_3^- at 1558 and 1270 cm^{-1} [59, 60], NO^+ at 2184 cm^{-1} [58, 60] and NO^- at 1186 cm^{-1} [58]. The bands between 2000 and 1700 cm^{-1} correspond to Ti^{3+}–NO, Ti^{4+}–NO [58], N_2O_3 [58, 60] and NO^+ [19]. The negative band at 1500 cm^{-1} may be connected with monodentate NO_3^- or NO_2^- [60].

In the second series of experiments with DRIFTS, the spectra were collected by averaging 5 scans. This decreased the signal-to-noise ratio and prevented the observation of most of the smaller peaks seen in Figure 16 (left), but enabled the collection of time series data on the most prominent band of NO_3^-. The left-hand panel of Figure 17 shows the time evolution of the absorption band, comparing the spectrum taken before O_3 production to spectra at 2 min and 12 min. The intensity of the band is presented on the right-hand panel of Figure 17 as a function of time, showing an initial quick increase and a subsequent stabilization. After the end of ozone production the intensity decreased and the absorption band disappeared in 10 minutes.

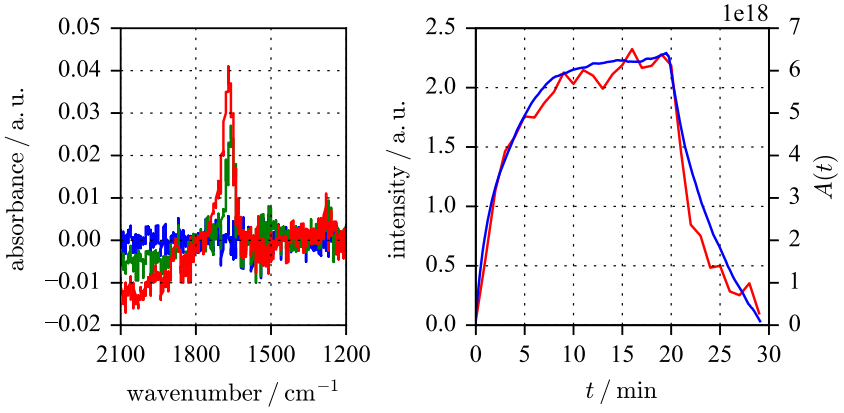

Figure 17. Results from DRIFTS measurements with 5 scans to average. On the left: NO_3^- absorption peak at 0 (in blue), 2 (in green), 12 (in red) min after the start of O_3 production. On the right: time-dependence of the intensity of the NO_3^- peak (in red), compared to the time-dependent adsorption function (18) (in blue).

For comparison, Figure 17 (right) also shows the time-dependent adsorption curve, based on the concentrations of gas-phase products and calculated by formula (18). It can be seen that the amount of adsorbed substance follows similar tendencies of quick initial increase, subsequent stabilization and drop to zero (i.e. desorption) after the end of ozone production. The similarities between the behaviors of the surface NO_3^- absorption band and the amounts of adsorbed or desorbed substances provide additional support for the conclusion that nitrate groups form on the catalyst surface during oxidation of NO_x by ozone.

Comparison of the NO_3^- absorption curves allows to estimate the influence of gas composition on the formation of NO_3^-. The DRIFTS measurement time series can be approximated by the function

$$f(t) = a\left[1 - \exp\left(-\frac{t}{\tau}\right)\right], \tag{19}$$

where a is the stabilized value of NO_3^- absorption band intensity and τ is the characteristic time of nitrate formation. In cases, where the gas phase concentration of NO_2 is approximately the same, the values of τ are observed to depend on the concentration of N_2O_5 in the gas phase according to an inversely proportional relationship (Figure 18). The results indicate faster saturation of NO_3^- formation at higher N_2O_5 concentrations, suggesting that direct absorption of N_2O_5 plays an important role in surface reaction mechanisms. The stabilized value a did not exhibit a notable dependence on $[N_2O_5]$.

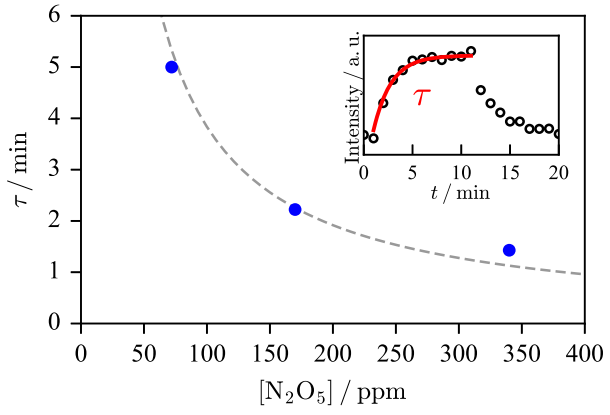

Figure 18. Characteristic time of NO_3^- formation on the surface of TiO_2 at different concentrations of N_2O_5 in the gas phase. The gas phase concentration of NO_2 was 50±10 ppm. The inset shows the modelling of an example measurement series by function (19).

5.3.3. Models of surface processes

In the following discussion about processes on the catalyst surfaces we first consider possible reaction pathways, based on results obtained in the NO_2 production regime. The characteristic time of reaction (12), which consumes O_3 on the oxidation of NO to NO_2, is below 10 ms [**II**]. On the other hand, estimates based on the geometry of the experimental setup indicate that the transition time from the mixing point of the O_2/O_3 and N_2/NO streams to the catalyst region is above 50 ms. Therefore, from the group of O_3, NO and NO_2, only NO and NO_2 can reach the surface of the catalyst. For this reason we consider models to describe the adsorption of NO_2 on the surface.

One possible mechanism, that has been proposed in literature, includes the adsorption of two NO_2 molecules, which then give rise to a surface-bound NO_3 and a gas-phase NO molecule [15, 61]:

$$2NO_2(s) \rightarrow NO_3(s) + NO(g). \tag{20}$$

According to this model, the ratio of consumed NO_2 to produced NO is 2.
In more recent works, a more complicated model of surface processes has been proposed for TiO_2 [19, 17], Al_2O_3 [14] and Cu-ZSM-5 [62]:

$$2NO_2(s) \leftrightarrow NO_3^-(s) + NO^+(s) \tag{21}$$

$$NO^+(s) + O^{2-}(s) \leftrightarrow NO_2^-(s) \tag{22}$$

$$NO_2^-(s) + NO_2(s) \leftrightarrow NO_3^-(s) + NO(g) \tag{23}$$

Reaction (21) is a disproportionation reaction, in which two adsorbed NO_2 molecules produce a nitrate ion NO_3^- and nitrosonium ion NO^+. The latter is highly reactive and incorporates a surface lattice oxygen O^{2-} in the production of a nitrite ion NO_2^-. The nitrite ion then reacts with another adsorbed NO_2 molecule, resulting in another NO_3^- and an NO molecule, which desorbs into the gas phase. These reactions can also proceed in the reverse directions. The net result of forward reactions is three adsorbed NO_2 molecules being converted to two NO_3^- ions and one NO molecule in the gas phase, so the above-mentioned ratio of consumed NO_2 to produced NO is 3.

This ratio can be determined for our experiments by analyzing the time dependencies of the outlet concentrations of NO and NO_2 at the beginning of ozone production (e.g. as seen in Figure 9c). Specifically, we investigate the quantities $\Delta[NO]$ and $\Delta[NO_2]$, i.e. the differences between the concentrations of NO or NO_2 at a given time instance and their corresponding stabilized values. Figure 19 presents two typical examples of these concentration differences as functions of time, both at the beginning and at after the end of ozone

production. Starting from either the switch-on or the switch-off of the ozone generator, the curves coincide if Δ[NO] is multiplied by a constant. This constant has the value of the above-mentioned ratio and in the given example is equal to 2.66 at the beginning and 3.23 after the end of ozone production. Data from other experiments indicates the same tendency of the ratio being closer to the value 3 instead of 2.

The model (21)–(23) is therefore in better agreement with our experimental data on gas-phase concentrations and is further reinforced by DRIFTS measurements, which identified NO_3^- as the main component of surface species. The model does not describe catalytic effects, but such effects were also not observed in our experiments in the NO_2 production regime (section 5.2.3).

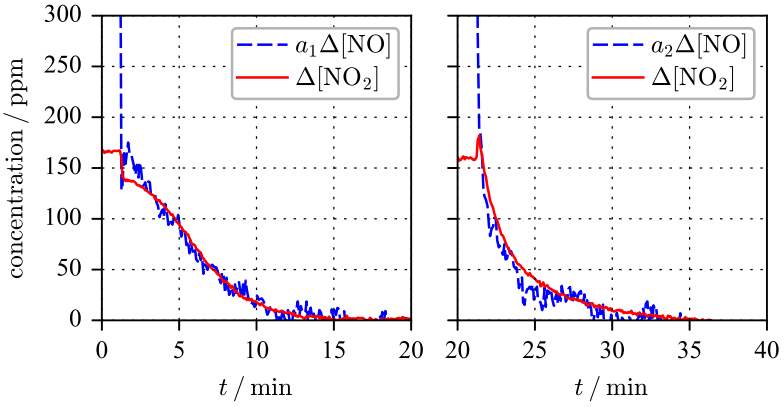

Figure 19. Comparison of changes in NO and NO_2 outlet concentrations at the beginning and following the end of ozone production. Experimental parameters: $[NO]_0$ = 400 ppm, T = 100 °C, flow rate 1 L/min, $[O_3]_0$ = 175 ppm. TiO_2 was used as catalyst. The values of parameters: a_1 = 2.66, a_2 = 3.23.

When the system is working in the N_2O_5 production regime ($[O_3]_0 > [NO]_0$), the conditions on the surface become significantly different due to the fact that ozone, that is left over from reaction (12), is now able to reach the surface of the catalyst. In our publications [**I–V**] we have proposed the following reaction mechanism to explain the experimental findings.

Simultaneously with the gas-phase NO_2 oxidation reaction (13), a fraction of the surplus O_3 reaches the catalyst surface and undergoes decomposition, leaving a supply of atomic oxygen on the surface:

$$O_3(g) + (s) \rightarrow O(s) + O_2(g). \qquad (24)$$

Ozone decomposition was experimentally investigated and is described in section 5.2.4. The process was most efficient on Fe_2O_3 and its rate increased with temperature.

The atomic oxygen on the surface can function as an additional oxidizing agent that converts adsorbed NO_2 molecules into NO_3:

$$NO_2(s) + O(s) \rightarrow NO_3(s). \quad (25)$$

Fe_2O_3, which was the most effective metal oxide in producing O-radicals on the surface, was also the best oxidizer of NO_2, suggesting a causal link between these properties. NO_3 can be the precursor of additional reactions, including the formation of N_2O_5, which has been proposed for atmospheric mineral dust surrogates. In this case, N_2O_5 may then desorb into the gas phase [63, 64]:

$$NO_3(s) + NO_2(g) \rightarrow N_2O_5(s), \quad (26)$$

$$N_2O_5(s) \leftrightarrow N_2O_5(g). \quad (27)$$

At the same time, reaction (27) can also proceed in the reverse direction and the increase in the quantities of surface species seen in Figure 15 is best explained by the simultaneous occurrence of ozone decomposition and direct adsorption of N_2O_5.

Since gas-phase N_2O_5 was not detected in the NO_2 production regime, this model suggests that NO_3 formed in reaction (25) is different from NO_3^- that is produced in reactions (21) and (23). This is consistent with the shift of the NO_3^- absorption band towards higher wavenumbers, as seen in Figure 16 (left).

The proposed model could explain two additional experimental findings that are seen in Figure 9. First, the peak in NO_2 outlet concentration after the end of ozone production occurred in case of all studied catalysts in the N_2O_5 regime and can be accounted for by the dynamic balance of forward and backward directions of reactions (21)–(23) and (26)–(27). With a constant flow of NO_2 reaching the surface, the direction with the end result of N_2O_5 formation is dominant. When the NO_2 flow to the surface stops, the balance shifts towards the generation of NO_2 until the supply of reversibly adsorbed NO_3 is depleted.

Reactions happening in reverse directions could also contribute to another interesting phenomenon, noted in Figure 9d, which is the absence of NO in the outlet between the moments of turning off the plasma reactor and the disappearance of N_2O_5. In addition to the reverse reactions (21)–(23), NO can also react with atomic oxygen on the surface, producing NO_2. At the same time, additional gas-phase NO_2 could shift the balance of reaction (26) towards the production of additional N_2O_5.

6. OPEN PROBLEMS

There are several potential directions for further research, concerning both the analysis of fundamental processes and questions regarding possible applications.

In the analysis of surface processes it was observed that nitrogen oxides remain on the surface as NO_3, but the amount of adsorbed species increased to a several times higher value, when the system transitioned from the NO_2 production regime to the N_2O_5 production regime. It is possible that additional adsorption sites become available, however further studies are needed to confirm that. For this purpose, additional experimental techniques could be applied, including temperature programmed desorption (TPD) and x-ray photoelectron spectroscopy (XPS). In case of XPS, for example, identification of surface compounds and their quantities, as well as information on local bonding of atoms would be possible.

Further verification of surface process mechanisms would be provided by reconstructing the experimental setup so that it is possible to achieve complete oxidation of NO_2 to N_2O_5 without producing any leftover ozone that could reach the catalyst surface. In that case any direct adsorption of N_2O_5 on the catalyst could be observed if it occurs.

In the current work, dry air conditions were simulated by the usage of N_2 and O_2 mixtures. However, fuel combustion exhausts also include water vapor, the influence of which should be investigated in future studies. The presence of water vapor is expected to result in the formation of HNO_3 instead of N_2O_5 as the final product. Blocking a fraction of adsorption sites is also a possible consequence.

Questions related to scaling up the process are important in view of potential application of the investigated NO_x removal method. Among these, increasing the amount of catalyst powder should be investigated, as the total surface area would be increased. To that end, the process of catalyst placement requires additional development, as mechanical pressing which is applied in this work, is likely not well scalable.

7. SUMMARY

In the current thesis, oxidation of NO_x in N_2 and O_2 mixtures was investigated, using the combined effects of plasma-generated species and metal oxide catalysts. Studies were carried out both in one-stage system, using direct oxidation by plasma, and two-stage system, applying oxidation by plasma-generated ozone. Dielectric-barrier discharge was used for the generation of plasma and nanoscale powder of TiO_2, γ-Al_2O_3 or γ-Fe_2O_3 was pressed on the inner wall of the reaction chamber. The aims of the work were to compare the effect of metal oxides on the efficiency of NO_x oxidation at different system configurations and temperatures, as well as determining the reaction mechanisms on the catalyst surface.

The efficiency of direct oxidation of NO by plasma was limited because of the occurrence of the back-reaction, mediated by O-radicals. The effect of catalyst was also limited, reaching a 35% increase in NO removal degree in case of Fe_2O_3 at 110 °C and 360 ppm of NO at the inlet. An exponential function of the specific input energy was used as an empirical model of the process, taking into account the effect of catalyst.

Oxidation of NO to NO_2 by ozone, lacking the direct influence of O-radicals in the gas phase, was much more efficient than direct oxidation by plasma, and enabled further oxidation of NO_2 to N_2O_5. The effective rate coefficient was defined to characterize the efficiency of the oxidation process. At temperatures above 80 °C, the metal oxide powders were found to increase the effective rate coefficient. The greatest improvement was achieved at 100 °C with Fe_2O_3, which increased the effective rate coefficient by a factor of 3, compared to oxidation only by ozone. The metal oxides were also shown to have an ozone degrading influence, with Fe_2O_3 active already at room temperature.

Two different approaches were taken to investigate reactions on the surfaces of the metal oxides. The analysis of time dependence of the outlet gas concentrations and direct monitoring of surface species by DRIFTS technique both confirmed that during oxidation by ozone, NO_2 undergoes adsorption and remains on the surface in the form of NO_3. The total amount of adsorbed species depends on the gas composition above the catalyst.

To explain the results, surface reaction pathways are proposed. A key component that accounts for the influence of metal oxides, is the decomposition of ozone on the surface of the metal oxides, resulting in a supply of atomic oxygen on the surface. Instead of the detrimental effect observed in the gas phase, surface-bound O-radicals initiate beneficial oxidation reactions that increase the efficiency of the overall process.

8. SUMMARY IN ESTONIAN

Katalüsaatorite toime lämmastikoksiidide oksüdeerimisel plasmaühenditega

Käesolevas doktoritöös uuriti lämmastikoksiidide (NO_x) oksüdeerimist N_2 ja O_2 segudes, kasutades plasmaühendite ja metalloksiidide koosmõju. Uuringud viidi läbi nii üheastmelises süsteemis, kasutades otsest plasmaga oksüdeerimist, kui ka kaheastmelises süsteemis, rakendades oksüdeerimist plasmas tekitatud osooniga. Plasma tekitamiseks kasutati dielektrikbarjäärlahendust ja samal ajal oli reaktsioonikambri siseseinale asetatud TiO_2, γ-Al_2O_3 või γ-Fe_2O_3 nanopulber. Töö eesmärkideks olid metalloksiidide mõju võrdlemine NO_x oksüdeerimisele erinevate süsteemi konfiguratsioonide ja temperatuuride korral, samuti katalüsaatori pinnal toimuvate protsesside väljaselgitamine.

NO otsene oksüdeerimine plasma abil oli piiratud hapnikuradikaalide osalusel toimuva pöördreaktsiooni poolt. Samuti oli piiratud katalüsaatori mõju, mis suurendas NO eemaldamise määra 35%, kui katalüsaatorina oli kasutusel Fe_2O_3, temperatuur oli 110 °C ja NO sisendkontsentratsioon 360 ppm. Kogu protsessi kirjeldamise empiirilise mudelina kasutati sisendenergia eksponentfunktsiooni, mis võttis arvesse ka katalüsaatori mõju.

NO oksüdeerimine NO_2-ks ainult osooni abil, mille korral puudus gaasifaasis hapnikuradikaalide mõju, oli otsesest plasmaoksüdeerimisest oluliselt efektiivsem ja võimaldas NO_2 edasist oksüdeerimist N_2O_5-ks. Kogu oksüdeerimisprotsessi iseloomustamiseks defineeriti efektiivne kiiruskonstant, mille väärtusi suurendasid metalloksiidid temperatuuridel üle 80 °C. Tugevaim mõju saavutati 100 °C juures Fe_2O_3 abil, mis tõi kaasa efektiivse kiiruskonstandi kolmekordse kasvu, võrreldes ainult osooni abil oksüdeerimisega. Metalloksiidid omasid ka osooni lagundavat mõju, kusjuures Fe_2O_3 oli selles osas aktiivne juba toatemperatuuril.

Metalloksiidide pinnal toimuvate protsesside uurimiseks kasutati kahte erinevat lähenemist. Nii väljundgaaside kontsentratsioonide ajaliste sõltuvuste analüüs kui ka pinna otsene jälgimine DRIFTS-meetodil näitasid, et osooniga oksüdeerimise ajal leiab aset NO_2 adsorptsioon ja lämmastikoksiidid püsivad pinnal NO_3 kujul. Pinnaühendite koguhulk sõltub gaasi koostisest katalüsaatori kohal.

Tulemuste seletamiseks on välja pakutud pinnareaktsioonide mehhanismid. Võtmetähtsusega protsess, mis selgitab metalloksiidide mõju, on osooni lagunemine metalloksiidi pinnal, mille tulemusel tekib sellel atomaarne hapnik. Efektiivsust vähendava mõju asemel, mis avalduks gaasifaasis, algatavad hapnikuradikaalid pinnal täiendavaid oksüdeerimisreaktsioone, mis suurendavad kogu protsessi efektiivsust.

REFERENCES

[1] I. Boscarato, N. Hickey, J. Kašpar, M. V. Prati and A. Mariani, Green shipping: Marine engine pollution abatement using a combined catalyst/seawater scrubber system. 1. Effect of catalyst, *J. Catal.* **328** (2015), 248–257.

[2] A. A. May, N. T. Nguyen, A. A. Presto, T. D. Gordon, E. M. Lipsky, M. Karve, A. Gutierrez, W. H. Robertson, M. Zhang, C. Brandow, O. Chang, S. Chen, P. Cicero-Fernandez, L. Dinkins, M. Fuentes, S.-M. Huang, R. Ling, J. Long, C. Maddox, J. Massetti, E. McCauley, A. Miguel, K. Na, R. Ong, Y. Pang, P. Rieger, T. Sax, T. Truong, T. Vo, S. Chattopadhyay, H. Maldonado, M. M. Maricq and A. L. Robinson, Gas- and particle-phase primary emissions from in-use, on-road gasoline and diesel vehicles, *Atmos. Environ.* **88** (2014), 247–260.

[3] R. J. Wild, W. P. Dubé, K. C. Aikin, S. J. Eilerman, J. A. Neuman, J. Peischl, T. B. Ryerson and S. S. Brown, On-road measurements of vehicle NO_2/NO_x emission ratios in Denver, Colorado, USA, *Atmos. Environ.* **148** (2017), 182–189.

[4] K. Skalska, J. S. Miller and S. Ledakowicz, Trends in NO_x abatement: A review, *Sci. Total Environ.* **408** (2010), 3976–3989.

[5] M. Kampa and E. Castanas, Human health effects of air pollution, *Environ. Pollut.* **151** (2008), 362–367.

[6] W. S. Epling, L. E. Campbell, A. Yezerets, N. W. Currier and J. E. Parks, Overview of the Fundamental Reactions and Degradation Mechanisms of NO_x Storage/Reduction Catalysts, *Catal. Rev.* **46** (2004), 163–245.

[7] B. M. Penetrante, M. C. Hsiao, B. T. Merritt and G. E. Vogtlin, Fundamental Limits on NO_x Reduction by Plasma, *J. Fuels Lubr.* **106** (1997), 737–740.

[8] B. Eliasson, M. Hirth and U. Kogelschatz, Ozone synthesis from oxygen in dielectric barrier discharges, *J. Phys. Appl. Phys.* **20** (1987), 1421.

[9] B. Eliasson and U. Kogelschatz, Modeling and applications of silent discharge plasmas, *IEEE Trans. Plasma Sci.* **19** (1991), 309–323.

[10] A. E. Wallis, J. C. Whitehead and K. Zhang, Plasma-assisted catalysis for the destruction of CFC-12 in atmospheric pressure gas streams using TiO_2, *Catal. Lett.* **113** (2007), 29–33.

[11] K. Hensel, Microdischarges in ceramic foams and honeycombs, *Eur. Phys. J. D* **54** (2009), 141–148.

[12] M. Kraus, B. Eliasson, U. Kogelschatz and A. Wokaun, CO_2 reforming of methane by the combination of dielectric-barrier discharges and catalysis, *Phys. Chem. Chem. Phys.* **3** (2001), 294–300.

[13] J. C. Whitehead, Plasma–catalysis: the known knowns, the known unknowns and the unknown unknowns, *J. Phys. Appl. Phys.* **49** (2016), 243001.

[14] N. Apostolescu, T. Schröder and S. Kureti, Study on the mechanism of the reaction of NO_2 with aluminium oxide, *Appl. Catal. B Environ.* **51** (2004), 43–50.

[15] J. Haubrich, R. G. Quiller, L. Benz, Z. Liu and C. M. Friend, In Situ Ambient Pressure Studies of the Chemistry of NO_2 and Water on Rutile TiO_2(110), *Langmuir* **26** (2010), 2445–2451.

[16] B. C. Hixson, J. W. Jordan, E. L. Wagner and H. M. Bevsek, Reaction Products and Kinetics of the Reaction of NO_2 with γ-Fe_2O_3, *J. Phys. Chem. A* **115** (2011), 13364–13369.

[17] L. Sivachandiran, F. Thevenet, P. Gravejat and A. Rousseau, Investigation of NO and NO_2 adsorption mechanisms on TiO_2 at room temperature, *Appl. Catal. B Environ.* **142–143** (2013), 196–204.

[18] O. Rosseler, M. Sleiman, V. N. Montesinos, A. Shavorskiy, V. Keller, N. Keller, M. I. Litter, H. Bluhm, M. Salmeron and H. Destaillats, Chemistry of NO_x on TiO_2 Surfaces Studied by Ambient Pressure XPS: Products, Effect of UV Irradiation, Water, and Coadsorbed K^+, *J. Phys. Chem. Lett.* **4** (2013), 536–541.
[19] L. Sivachandiran, F. Thevenet, A. Rousseau and D. Bianchi, NO_2 adsorption mechanism on TiO_2: An in-situ transmission infrared spectroscopy study, *Appl. Catal. B Environ.* **198** (2016), 411–419.
[20] E. A. Davidson and W. Kingerlee, A global inventory of nitric oxide emissions from soils, *Nutr. Cycl. Agroecosystems* **48** (1997), 37–50.
[21] J. N. Galloway, F. J. Dentener, D. G. Capone, E. W. Boyer, R. W. Howarth, S. P. Seitzinger, G. P. Asner, C. C. Cleveland, P. A. Green, E. A. Holland, D. M. Karl, A. F. Michaels, J. H. Porter, A. R. Townsend and C. J. Vörösmarty, Nitrogen Cycles: Past, Present, and Future, *Biogeochemistry* **70** (2004), 153–226.
[22] L. T. Murray, Lightning NO_x and Impacts on Air Quality, *Curr. Pollut. Rep.* **2** (2016), 115–133.
[23] G. E. Likens, C. T. Driscoll and D. C. Buso, Long-Term Effects of Acid Rain: Response and Recovery of a Forest Ecosystem, *Science* **272** (1996), 244–246.
[24] C. Potera, Air Pollution: Salt Mist Is the Right Seasoning for Ozone, *Environ. Health Perspect.* **116** (2008), A288.
[25] Commission Regulation (EU) No 459/2012 of 29 May 2012 amending Regulation (EC) No 715/2007 of the European Parliament and of the Council and Commission Regulation (EC) No 692/2008 as regards emissions from light passenger and commercial vehicles (Euro 6), Eur-lex.europa.eu.
[26] Directive 2010/75/EU of the European Parliament and of the Council of 24 November 2010 on Industrial Emissions (Integrated Pollution Prevention and Control) (2010).
[27] International Maritime Organization Prevention of Air Pollution from Ships, http://imo.org/en/OurWork/environment/pollutionprevention/airpollution/pages/air-pollution.aspx.
[28] W. Duo, K. Dam□Johansen and K. Østergaard, Kinetics of the gas-phase reaction between nitric oxide, ammonia and oxygen, *Can. J. Chem. Eng.* **70** (1992), 1014–1020.
[29] M. Laroussi and T. Akan, Arc-Free Atmospheric Pressure Cold Plasma Jets: A Review, *Plasma Process. Polym.* **4** (2007), 777–718.
[30] J. Niu, B. Peng, Q. Yang, Y. Cong, D. Liu and H. Fan, Spectroscopic diagnostics of plasma-assisted catalytic systems for NO removal from $NO/N_2/O_2/C_2H_4$ mixtures, *Catal. Today* **211** (2013), 58–65.
[31] A. Fridman, S. Nester, L. A. Kennedy, A. Saveliev and O. Mutaf-Yardimci, Gliding arc gas discharge, *Prog. Energy Combust. Sci.* **25** (1999), 211–231.
[32] H. D. Stryczewska, T. Jakubowski, S. Kalisiak, T. Giżewski and J. Pawłat, Power Systems of Plasma Reactors for Non-Thermal Plasma Generation, *J. Adv. Oxid. Technol.* **16** (2016), 52–62.
[33] T. C. Manley, The Electric Characteristics of the Ozonator Discharge, *Trans. Electrochem. Soc.* **84** (1943), 83–96.
[34] Z. Falkenstein and J. J. Coogan, Microdischarge behaviour in the silent discharge of nitrogen-oxygen and water-air mixtures, *J. Phys. Appl. Phys.* **30** (1997), 817.
[35] F. Arsac, D. Bianchi, J. M. Chovelon, C. Ferronato and J. M. Herrmann, Experimental Microkinetic Approach of the Photocatalytic Oxidation of Isopropyl

Alcohol on TiO_2. Part 1. Surface Elementary Steps Involving Gaseous and Adsorbed C_3H_x O Species, *J. Phys. Chem. A* **110** (2006), 4202–4212.
[36] S. Pekárek, J. Mikeš, I. Beshajová Pelikánová, F. Krčma and P. Dzik, Effect of TiO_2 on Various Regions of Active Electrode on Surface Dielectric Barrier Discharge in Air, *Plasma Chem. Plasma Process.* **36** (2016), 1187–1200.
[37] X. Tu, H. J. Gallon and J. C. Whitehead, Dynamic Behavior of an Atmospheric Argon Gliding Arc Plasma, *IEEE Trans. Plasma Sci.* **39** (2011), 2900–2901.
[38] X. Tu, H. J. Gallon and J. C. Whitehead, Electrical and spectroscopic diagnostics of a single-stage plasma-catalysis system: effect of packing with TiO_2, *J. Phys. Appl. Phys.* **44** (2011), 482003.
[39] A. M. Harling, D. J. Glover, J. C. Whitehead and K. Zhang, The role of ozone in the plasma-catalytic destruction of environmental pollutants, *Appl. Catal. B Environ.* **90** (2009), 157–161.
[40] A. Ogata, K. Saito, H.-H. Kim, M. Sugasawa, H. Aritani and H. Einaga, Performance of an Ozone Decomposition Catalyst in Hybrid Plasma Reactors for Volatile Organic Compound Removal, *Plasma Chem. Plasma Process.* **30** (2010), 33–42.
[41] T. Hammer, Application of Plasma Technology in Environmental Techniques, *Contrib. Plasma Phys.* **39** (1999), 441–462.
[42] K. Yan, E. J. M. van Heesch, A. J. M. Pemen and P. A. H. J. Huijbrechts, From Chemical Kinetics to Streamer Corona Reactor and Voltage Pulse Generator, *Plasma Chem. Plasma Process.* **21** (2001), 107–137.
[43] L. A. Rosocha and R. A. Korzekwa, Removal of Volatile Organic Compounds (VOCs) by Atmospheric-Pressure Dielectric-Barrier and Pulsed-Corona Electrical Discharges, in *Electrical Discharges for Environmental Purposes: Scientific Background and Applications* (E. M. van Veldhuizen, editor), Nova Science (1999).
[44] H.-H. Kim, A. Ogata and S. Futamura, Atmospheric plasma-driven catalysis for the low temperature decomposition of dilute aromatic compounds, *J. Phys. Appl. Phys.* **38** (2005), 1292–1300.
[45] S. T. Oyama, Chemical and Catalytic Properties of Ozone, *Catal. Rev.* **42** (2000), 279–322.
[46] H.-H. Kim, Nonthermal Plasma Processing for Air-Pollution Control: A Historical Review, Current Issues, and Future Prospects, *Plasma Process. Polym.* **1** (2004), 91–110.
[47] I. Jõgi, A. Haljaste and M. Laan, Hybrid TiO_2 based plasma-catalytic reactors for the removal of hazardous gasses, *Surf. Coat. Technol.* **242** (2014), 195–199.
[48] H. H. Kim, K. Tsunoda, S. Katsura and A. Mizuno, A novel plasma reactor for NO_x control using photocatalyst and hydrogen peroxide injection, *IEEE Trans. Ind. Appl.* **35** (1999), 1306–1310.
[49] I. Jõgi, E. Levoll and J. Raud, Plasma oxidation of NO in O_2:N_2 mixtures: The importance of back-reaction, *Chem. Eng. J.* **301** (2016), 149–157.
[50] C. R. McLarnon and B. M. Penetrante, Effect of Gas Composition on the NO_x Conversion Chemistry in a Plasma, *Society of Automotive Engineers Fall Fuels and Lubricants Meeting*, San Francisco, CA (1998).
[51] B. Dhandapani and S. T. Oyama, Gas phase ozone decomposition catalysts, *Appl. Catal. B Environ.* **11** (1997), 129–166.
[52] H. Keller-Rudek, G. K. Moortgat, R. Sander and R. Sörensen, The MPI-Mainz UV/VIS Spectral Atlas of Gaseous Molecules of Atmospheric Interest, *Earth Syst. Sci. Data* **5** (2013), 365–373.

[53] I. Jõgi, K. Erme, E. Levoll and E. Stamate, Radical production efficiency and electrical characteristics of a coplanar barrier discharge built by multilayer ceramic technology, *J. Phys. Appl. Phys.* **50** (2017), 465201.
[54] NIST Chemical Kinetics Database, https://kinetics.nist.gov/kinetics/index.jsp (27 March 2019).
[55] B. M. Penetrante, R. M. Brusasco, B. T. Merritt, W. J. Pitz, G. E. Vogtlin, M. C. Kung, H. H. Kung, C. Z. Wan and K. E. Voss, Plasma-Assisted Catalytic Reduction of NO_x, *SAE Trans.* **107** (1998), 1222–1231.
[56] I. Jõgi, E. Levoll and J. Raud, Effect of Catalyst Placement on the Plasma-Catalytic Oxidation of NO, *Catal. Lett.* **147** (2017), 566–571.
[57] R. Atkinson, D. L. Baulch, R. A. Cox, J. N. Crowley, R. F. Hampson, R. G. Hynes, M. E. Jenkin, M. J. Rossi and J. Troe, Evaluated kinetic and photochemical data for atmospheric chemistry: Volume I – gas phase reactions of O_x, HO_x, NO_x and SO_x species, *Atmospheric Chem. Phys.* **4** (2004), 1461–1768.
[58] R. V. Mikhaylov, A. A. Lisachenko, B. N. Shelimov, V. B. Kazansky, G. Martra and S. Coluccia, FTIR and TPD Study of the Room Temperature Interaction of a NO–Oxygen Mixture and of NO_2 with Titanium Dioxide, *J. Phys. Chem. C* **117** (2013), 10345–10352.
[59] C. E. Nanayakkara, W. A. Larish and V. H. Grassian, Titanium Dioxide Nanoparticle Surface Reactivity with Atmospheric Gases, CO_2, SO_2, and NO_2: Roles of Surface Hydroxyl Groups and Adsorbed Water in the Formation and Stability of Adsorbed Products, *J. Phys. Chem. C* **118** (2014), 23011–23021.
[60] K. Hadjiivanov and H. Knözinger, Species formed after NO adsorption and NO+O_2 co-adsorption on TiO_2: an FTIR spectroscopic study, *Phys. Chem. Chem. Phys.* **2** (2000), 2803–2806.
[61] J. A. Rodriguez, T. Jirsak, G. Liu, J. Hrbek, J. Dvorak and A. Maiti, Chemistry of NO_2 on Oxide Surfaces: Formation of NO_3 on TiO_2(110) and NO_2↔O Vacancy Interactions, *J. Am. Chem. Soc.* **123** (2001), 9597–9605.
[62] L. Olsson, H. Sjövall and R. J. Blint, Detailed kinetic modeling of NO_x adsorption and NO oxidation over Cu-ZSM-5, *Appl. Catal. B Environ.* **87** (2009), 200–210.
[63] F. Karagulian and M. J. Rossi, The heterogeneous chemical kinetics of NO_3 on atmospheric mineral dust surrogates, *Phys. Chem. Chem. Phys.* **7** (2005), 3150.
[64] F. Karagulian and M. J. Rossi, Heterogeneous Chemistry of the NO_3 Free Radical and N_2O_5 on Decane Flame Soot at Ambient Temperature: Reaction Products and Kinetics, *J. Phys. Chem. A* **111** (2007), 1914–1926.

ACKNOWLEDGEMENTS

First of all, I would like to thank my supervisor Indrek Jõgi for support and guidance throughout the research. I am also grateful to all the members of the Plasma Physics Laboratory for their useful feedback. Special thanks to the laboratory engineer Tõnu Asu for preparing the metal oxide coatings that were used in our experiments.

This research was financed by the Estonian Science Foundation grant no. 9310 and Estonian Research Council grant no. 585. The research has been partially supported by ASTRA project PER ASPERA Graduate School of Functional Materials and Technologies receiving funding from the European Regional Development Fund under project in University of Tartu, Estonia

European Union
European Regional
Development Fund

Investing
in your future

PUBLICATIONS

CURRICULUM VITAE

Name: Kalev Erme
Date of birth: 9 February 1986
Nationality: Estonian
Phone: +372 5667 5655
E-mail: kalev.erme@ut.ee, kalev2@msn.com

Education

2005	Miina Härma Gymnasium
2012	University of Tartu, BSc in physics
2014	University of Tartu, MSc in physics (*cum laude*)

List of publications

- Jõgi, K. Erme, A. Haljaste, M. Laan, Oxidation of nitrogen oxide in hybrid plasma-catalytic reactors based on DBD and Fe_2O_3, *The European Physical Journal: Applied Physics*, 61 (2013) 24305.
- Jõgi, K. Erme, J. Raud, M. Laan, Oxidation of NO by ozone in the presence of TiO_2 catalyst, *Fuel*, 173 (2016) 45–51.
- Jõgi, K. Erme, E. Levoll, E. Stamate, Radical production efficiency and electrical characteristics of a coplanar barrier discharge built by multilayer ceramic technology, *Journal of Physics D: Applied Physics*, 50 (2017) 465201.
- K. Erme, J. Raud, I. Jõgi, Adsorption of Nitrogen Oxides on TiO_2 Surface as a Function of NO_2 and N_2O_5 Fraction in the Gas Phase, *Langmuir*, 34 (2018) 6338–6345.
- Jõgi, K. Erme, E. Levoll, J. Raud, E. Stamate, Plasma and catalyst for the oxidation of NO_x, *Plasma Sources Science and Technology*, 27 (2018) 035001.
- K. Erme, I. Jõgi, Metal Oxides as Catalysts and Adsorbents in Ozone Oxidation of NO_x, *Environmental Science & Technology*, 53 (2019) 5266–5271.

Conference presentations

- K. Erme, I. Jõgi. Ozone Enhanced Adsorption of Nitrogen-Oxides on TiO_2 Powders. EcoBalt 2016, Tartu, 9–12 October 2016.
- K. Erme, I. Jõgi, U. Püttsepp, E. Levoll, E. Stamate. Characterization of Coplanar Surface Barrier Discharge. Graduate School of Functional Materials and Technologies Scientific Conference 2017, Tartu, 7–8 March 2017.
- K. Erme, I. Jõgi. Removal of Nitrogen Oxides with Ozone and Metal Oxides. Graduate School of Functional Materials and Technologies Scientific Conference 2018, Tallinn, 7–8 March, 2018.
- K. Erme, I. Jõgi. The Effect of Catalyst on Ozone and Nitrous Oxide Production in Dielectric Barrier Discharge. 22nd Symposium on Application

of Plasma Processes and 11th EU-Japan Joint Symposium on Plasma Processing, Štrbske Pleso, Slovakia, 18–24 January 2019.

- K. Erme, I. Jõgi. Metal Oxides as Catalysts and Adsorbents in Ozone Oxidation of Nitrogen Oxides. Graduate School of Functional Materials and Technologies Scientific Conference 2019, Tartu, 4–5 February 2019.

ELULOOKIRJELDUS

Nimi: Kalev Erme
Sünniaeg: 9. veebruar 1986
Kodakondsus: Eesti
Telefon: +372 5667 5655
E-mail: kalev.erme@ut.ee, kalev2@msn.com

Haridus

2005	Miina Härma gümnaasium
2012	Tartu Ülikool, BSc füüsikas
2014	Tartu Ülikool, MSc füüsikas (*cum laude*)

Publikatsioonide loetelu

- Jõgi, K. Erme, A. Haljaste, M. Laan, Oxidation of nitrogen oxide in hybrid plasma-catalytic reactors based on DBD and Fe_2O_3, *The European Physical Journal: Applied Physics*, 61 (2013) 24305.
- Jõgi, K. Erme, J. Raud, M. Laan, Oxidation of NO by ozone in the presence of TiO_2 catalyst, *Fuel*, 173 (2016) 45–51.
- Jõgi, K. Erme, E. Levoll, E. Stamate, Radical production efficiency and electrical characteristics of a coplanar barrier discharge built by multilayer ceramic technology, *Journal of Physics D: Applied Physics*, 50 (2017) 465201.
- K. Erme, J. Raud, I. Jõgi, Adsorption of Nitrogen Oxides on TiO_2 Surface as a Function of NO_2 and N_2O_5 Fraction in the Gas Phase, *Langmuir*, 34 (2018) 6338–6345.
- Jõgi, K. Erme, E. Levoll, J. Raud, E. Stamate, Plasma and catalyst for the oxidation of NO_x, *Plasma Sources Science and Technology*, 27 (2018) 035001.
- K. Erme, I. Jõgi, Metal Oxides as Catalysts and Adsorbents in Ozone Oxidation of NO_x, *Environmental Science & Technology*, 53 (2019) 5266–5271.

Konverentsiettekanded

- K. Erme, I. Jõgi. Ozone Enhanced Adsorption of Nitrogen-Oxides on TiO_2 Powders. EcoBalt 2016, Tartu, 9.–12. oktoober 2016.
- K. Erme, I. Jõgi, U. Püttsepp, E. Levoll, E. Stamate. Characterization of Coplanar Surface Barrier Discharge. Funktsionaalsete materjalide ja tehnoloogiate doktorikooli teaduskonverents 2017, Tartu, 7.–8. märts 2017.
- K. Erme, I. Jõgi. Removal of Nitrogen Oxides with Ozone and Metal Oxides. Funktsionaalsete materjalide ja tehnoloogiate doktorikooli teaduskonverents 2018, Tallinn, 7.–8. märts, 2018.
- K. Erme, I. Jõgi. The Effect of Catalyst on Ozone and Nitrous Oxide Production in Dielectric Barrier Discharge. 22nd Symposium on Application of

Plasma Processes and 11th EU-Japan Joint Symposium on Plasma Processing, Štrbske Pleso, Slovakkia, 18.–24. jaanuar 2019.

- K. Erme, I. Jõgi. Metal Oxides as Catalysts and Adsorbents in Ozone Oxidation of Nitrogen Oxides. Funktsionaalsete materjalide ja tehnoloogiate doktorikooli teaduskonverents 2019, Tartu, 4.–5. veebruar 2019.

DISSERTATIONES PHYSICAE UNIVERSITATIS TARTUENSIS

1. **Andrus Ausmees.** XUV-induced electron emission and electron-phonon interaction in alkali halides. Tartu, 1991.
2. **Heiki Sõnajalg.** Shaping and recalling of light pulses by optical elements based on spectral hole burning. Tartu, 1991.
3. **Sergei Savihhin.** Ultrafast dynamics of F-centers and bound excitons from picosecond spectroscopy data. Tartu, 1991.
4. **Ergo Nõmmiste.** Leelishalogeniidide röntgenelektronemissioon kiiritamisel footonitega energiaga 70–140 eV. Tartu, 1991.
5. **Margus Rätsep.** Spectral gratings and their relaxation in some low-temperature impurity-doped glasses and crystals. Tartu, 1991.
6. **Tõnu Pullerits.** Primary energy transfer in photosynthesis. Model calculations. Tartu, 1991.
7. **Olev Saks.** Attoampri diapasoonis voolude mõõtmise füüsikalised alused. Tartu, 1991.
8. **Andres Virro.** AlGaAsSb/GaSb heterostructure injection lasers. Tartu, 1991.
9. **Hans Korge.** Investigation of negative point discharge in pure nitrogen at atmospheric pressure. Tartu, 1992.
10. **Jüri Maksimov.** Nonlinear generation of laser VUV radiation for high-resolution spectroscopy. Tartu, 1992.
11. **Mark Aizengendler.** Photostimulated transformation of aggregate defects and spectral hole burning in a neutron-irradiated sapphire. Tartu, 1992.
12. **Hele Siimon.** Atomic layer molecular beam epitaxy of A^2B^6 compounds described on the basis of kinetic equations model. Tartu, 1992.
13. **Tõnu Reinot.** The kinetics of polariton luminescence, energy transfer and relaxation in anthracene. Tartu, 1992.
14. **Toomas Rõõm.** Paramagnetic H^{2-} and F^+ centers in CaO crystals: spectra, relaxation and recombination luminescence. Tallinn, 1993.
15. **Erko Jalviste.** Laser spectroscopy of some jet-cooled organic molecules. Tartu, 1993.
16. **Alvo Aabloo.** Studies of crystalline celluloses using potential energy calculations. Tartu, 1994.
17. **Peeter Paris.** Initiation of corona pulses. Tartu, 1994.
18. **Павел Рубин.** Локальные дефектные состояния в CuO_2 плоскостях высокотемпературных сверхпроводников. Тарту, 1994.
19. **Olavi Ollikainen.** Applications of persistent spectral hole burning in ultrafast optical neural networks, time-resolved spectroscopy and holographic interferometry. Tartu, 1996.
20. **Ülo Mets.** Methodological aspects of fluorescence correlation spectroscopy. Tartu, 1996.
21. **Mikhail Danilkin.** Interaction of intrinsic and impurity defects in CaS:Eu luminophors. Tartu, 1997.

22. **Ирина Кудрявцева.** Создание и стабилизация дефектов в кристаллах KBr, KCl, RbCl при облучении ВУФ-радиацией. Тарту, 1997.
23. **Andres Osvet.** Photochromic properties of radiation-induced defects in diamond. Tartu, 1998.
24. **Jüri Örd.** Classical and quantum aspects of geodesic multiplication. Tartu, 1998.
25. **Priit Sarv.** High resolution solid-state NMR studies of zeolites. Tartu, 1998.
26. **Сергей Долгов.** Электронные возбуждения и дефектообразование в некоторых оксидах металлов. Тарту, 1998.
27. **Kaupo Kukli.** Atomic layer deposition of artificially structured dielectric materials. Tartu, 1999.
28. **Ivo Heinmaa.** Nuclear resonance studies of local structure in $RBa_2Cu_3O_{6+x}$ compounds. Tartu, 1999.
29. **Aleksander Shelkan.** Hole states in CuO_2 planes of high temperature superconducting materials. Tartu, 1999.
30. **Dmitri Nevedrov.** Nonlinear effects in quantum lattices. Tartu, 1999.
31. **Rein Ruus.** Collapse of 3d (4f) orbitals in 2p (3d) excited configurations and its effect on the x-ray and electron spectra. Tartu, 1999.
32. **Valter Zazubovich.** Local relaxation in incommensurate and glassy solids studied by Spectral Hole Burning. Tartu, 1999.
33. **Indrek Reimand.** Picosecond dynamics of optical excitations in GaAs and other excitonic systems. Tartu, 2000.
34. **Vladimir Babin.** Spectroscopy of exciton states in some halide macro- and nanocrystals. Tartu, 2001.
35. **Toomas Plank.** Positive corona at combined DC and AC voltage. Tartu, 2001.
36. **Kristjan Leiger.** Pressure-induced effects in inhomogeneous spectra of doped solids. Tartu, 2002.
37. **Helle Kaasik.** Nonperturbative theory of multiphonon vibrational relaxation and nonradiative transitions. Tartu, 2002.
38. **Tõnu Laas.** Propagation of waves in curved spacetimes. Tartu, 2002.
39. **Rünno Lõhmus.** Application of novel hybrid methods in SPM studies of nanostructural materials. Tartu, 2002.
40. **Kaido Reivelt.** Optical implementation of propagation-invariant pulsed free-space wave fields. Tartu, 2003.
41. **Heiki Kasemägi.** The effect of nanoparticle additives on lithium-ion mobility in a polymer electrolyte. Tartu, 2003.
42. **Villu Repän.** Low current mode of negative corona. Tartu, 2004.
43. **Алексей Котлов.** Оксианионные диэлектрические кристаллы: зонная структура и электронные возбуждения. Tartu, 2004.
44. **Jaak Talts.** Continuous non-invasive blood pressure measurement: comparative and methodological studies of the differential servo-oscillometric method. Tartu, 2004.
45. **Margus Saal.** Studies of pre-big bang and braneworld cosmology. Tartu, 2004.

46. **Eduard Gerškevitš.** Dose to bone marrow and leukaemia risk in external beam radiotherapy of prostate cancer. Tartu, 2005.
47. **Sergey Shchemelyov.** Sum-frequency generation and multiphoton ionization in xenon under excitation by conical laser beams. Tartu, 2006.
48. **Valter Kiisk.** Optical investigation of metal-oxide thin films. Tartu, 2006.
49. **Jaan Aarik.** Atomic layer deposition of titanium, zirconium and hafnium dioxides: growth mechanisms and properties of thin films. Tartu, 2007.
50. **Astrid Rekker.** Colored-noise-controlled anomalous transport and phase transitions in complex systems. Tartu, 2007.
51. **Andres Punning.** Electromechanical characterization of ionic polymer-metal composite sensing actuators. Tartu, 2007.
52. **Indrek Jõgi.** Conduction mechanisms in thin atomic layer deposited films containing TiO_2. Tartu, 2007.
53. **Aleksei Krasnikov.** Luminescence and defects creation processes in lead tungstate crystals. Tartu, 2007.
54. **Küllike Rägo.** Superconducting properties of MgB_2 in a scenario with intra- and interband pairing channels. Tartu, 2008.
55. **Els Heinsalu.** Normal and anomalously slow diffusion under external fields. Tartu, 2008.
56. **Kuno Kooser.** Soft x-ray induced radiative and nonradiative core-hole decay processes in thin films and solids. Tartu, 2008.
57. **Vadim Boltrushko.** Theory of vibronic transitions with strong nonlinear vibronic interaction in solids. Tartu, 2008.
58. **Andi Hektor.** Neutrino Physics beyond the Standard Model. Tartu, 2008.
59. **Raavo Josepson.** Photoinduced field-assisted electron emission into gases. Tartu, 2008.
60. **Martti Pärs.** Study of spontaneous and photoinduced processes in molecular solids using high-resolution optical spectroscopy. Tartu, 2008.
61. **Kristjan Kannike.** Implications of neutrino masses. Tartu, 2008.
62. **Vigen Issahhanjan.** Hole and interstitial centres in radiation-resistant MgO single crystals. Tartu, 2008.
63. **Veera Krasnenko.** Computational modeling of fluorescent proteins. Tartu, 2008.
64. **Mait Müntel.** Detection of doubly charged higgs boson in the CMS detector. Tartu, 2008.
65. **Kalle Kepler.** Optimisation of patient doses and image quality in diagnostic radiology. Tartu, 2009.
66. **Jüri Raud.** Study of negative glow and positive column regions of capillary HF discharge. Tartu, 2009.
67. **Sven Lange.** Spectroscopic and phase-stabilisation properties of pure and rare-earth ions activated ZrO_2 and HfO_2. Tartu, 2010.
68. **Aarne Kasikov.** Optical characterization of inhomogeneous thin films. Tartu, 2010.
69. **Heli Valtna-Lukner.** Superluminally propagating localized optical pulses. Tartu, 2010.

70. **Artjom Vargunin.** Stochastic and deterministic features of ordering in the systems with a phase transition. Tartu, 2010.
71. **Hannes Liivat.** Probing new physics in e+e− annihilations into heavy particles via spin orientation effects. Tartu, 2010.
72. **Tanel Mullari.** On the second order relativistic deviation equation and its applications. Tartu, 2010.
73. **Aleksandr Lissovski.** Pulsed high-pressure discharge in argon: spectroscopic diagnostics, modeling and development. Tartu, 2010.
74. **Aile Tamm.** Atomic layer deposition of high-permittivity insulators from cyclopentadienyl-based precursors. Tartu, 2010.
75. **Janek Uin.** Electrical separation for generating standard aerosols in a wide particle size range. Tartu, 2011.
76. **Svetlana Ganina.** Hajusandmetega ülesanded kui üks võimalus füüsikaõppe efektiivsuse tõstmiseks. Tartu, 2011
77. **Joel Kuusk.** Measurement of top-of-canopy spectral reflectance of forests for developing vegetation radiative transfer models. Tartu, 2011.
78. **Raul Rammula**. Atomic layer deposition of HfO_2 – nucleation, growth and structure development of thin films. Tartu, 2011.
79. **Сергей Наконечный.** Исследование электронно-дырочных и интерстициал-вакансионных процессов в монокристаллах MgO и LiF методами термоактивационной спектроскопии. Тарту, 2011.
80. **Niina Voropajeva.** Elementary excitations near the boundary of a strongly correlated crystal. Tartu, 2011.
81. **Martin Timusk.** Development and characterization of hybrid electro-optical materials. Tartu, 2012, 106 p.
82. **Merle Lust.** Assessment of dose components to Estonian population. Tartu, 2012, 84 p.
83. **Karl Kruusamäe.** Deformation-dependent electrode impedance of ionic electromechanically active polymers. Tartu, 2012, 128 p.
84. **Liis Rebane.** Measurement of the $W \to \tau\nu$ cross section and a search for a doubly charged Higgs boson decaying to τ-leptons with the CMS detector. Tartu, 2012, 156 p.
85. **Jevgeni Šablonin.** Processes of structural defect creation in pure and doped MgO and NaCl single crystals under condition of low or super high density of electronic excitations. Tartu, 2013, 145 p.
86. **Riho Vendt**. Combined method for establishment and dissemination of the international temperature scale. Tartu, 2013, 108 p.
87. **Peeter Piksarv.** Spatiotemporal characterization of diffractive and non-diffractive light pulses. Tartu, 2013, 156 p.
88. **Anna Šugai.** Creation of structural defects under superhigh-dense irradiation of wide-gap metal oxides. Tartu, 2013, 108 p.
89. **Ivar Kuusik.** Soft X-ray spectroscopy of insulators. Tartu, 2013, 113 p.
90. **Viktor Vabson**. Measurement uncertainty in Estonian Standard Laboratory for Mass. Tartu, 2013, 134 p.

91. **Kaupo Voormansik.** X-band synthetic aperture radar applications for environmental monitoring. Tartu, 2014, 117 p.
92. **Deivid Pugal.** hp-FEM model of IPMC deformation. Tartu, 2014, 143 p.
93. **Siim Pikker.** Modification in the emission and spectral shape of photostable fluorophores by nanometallic structures. Tartu, 2014, 98 p.
94. **Mihkel Pajusalu**. Localized Photosynthetic Excitons. Tartu, 2014, 183 p.
95. **Taavi Vaikjärv.** Consideration of non-adiabaticity of the Pseudo-Jahn-Teller effect: contribution of phonons. Tartu, 2014, 129 p.
96. **Martin Vilbaste.** Uncertainty sources and analysis methods in realizing SI units of air humidity in Estonia. Tartu, 2014, 111 p.
97. **Mihkel Rähn.** Experimental nanophotonics: single-photon sources- and nanofiber-related studies. Tartu, 2015, 107 p.
98. **Raul Laasner.** Excited state dynamics under high excitation densities in tungstates. Tartu, 2015, 125 p.
99. **Andris Slavinskis.** EST Cube-1 attitude determination. Tartu, 2015, 104 p.
100. **Karlis Zalite**. Radar Remote Sensing for Monitoring Forest Floods and Agricultural Grasslands. Tartu, 2016, 124 p.
101. **Kaarel Piip.** Development of LIBS for *in-situ* study of ITER relevant materials. Tartu, 2016, 93 p.
102. **Kadri Isakar.** ^{210}Pb in Estonian air: long term study of activity concentrations and origin of radioactive lead. Tartu, 2016, 107 p.
103. **Artur Tamm.** High entropy alloys: study of structural properties and irradiation response. Tartu, 2016, 115 p.
104. **Rasmus Talviste.** Atmospheric-pressure He plasma jet: effect of dielectric tube diameter. Tartu, 2016, 107 p.
105. **Andres Tiko.** Measurement of single top quark properties with the CMS detector. Tartu, 2016, 161 p.
106. **Aire Olesk.** Hemiboreal Forest Mapping with Interferometric Synthetic Aperture Radar. Tartu, 2016, 121 p.
107. **Fred Valk.** Nitrogen emission spectrum as a measure of electric field strength in low-temperature gas discharges. Tartu, 2016, 149 p.
108. **Manoop Chenchiliyan.** Nano-structural Constraints for the Picosecond Excitation Energy Migration and Trapping in Photosynthetic Membranes of Bacteria. Tartu, 2016, 115p.
109. **Lauri Kaldamäe.** Fermion mass and spin polarisation effects in top quark pair production and the decay of the higgs boson. Tartu, 2017, 104 p.
110. **Marek Oja.** Investigation of nano-size α- and transition alumina by means of VUV and cathodoluminescence spectroscopy. Tartu, 2017, 89 p.
111. **Viktoriia Levushkina.** Energy transfer processes in the solid solutions of complex oxides. Tartu, 2017, 101 p.
112. **Mikk Antsov.** Tribomechanical properties of individual 1D nanostructures: experimental measurements supported by finite element method simulations. Tartu, 2017, 101 p.
113. **Hardi Veermäe.** Dark matter with long range vector-mediated interactions. Tartu, 2017, 137 p.

114. **Aris Auzans.** Development of computational model for nuclear energy systems analysis: natural resources optimisation and radiological impact minimization. Tartu, 2018, 138 p.
115. **Aleksandr Gurev**. Coherent fluctuating nephelometry application in laboratory practice. Tartu, 2018, 150 p.
116. **Ardi Loot**. Enhanced spontaneous parametric downconversion in plasmonic and dielectric structures. Tartu, 2018, 164 p.
117. **Andreas Valdmann.** Generation and characterization of accelerating light pulses. Tartu, 2019, 85 p.
118. **Mikk Vahtrus.** Structure-dependent mechanical properties of individual one-dimensional metal-oxide nanostructures. Tartu, 2019, 110 p.
119. **Ott Vilson.** Transformation properties and invariants in scalar-tensor theories of gravity. Tartu, 2019, 183 p.
120. **Indrek Sünter.** Design and characterisation of subsystems and software for ESTCube-1 nanosatellite. Tartu, 2019, 195 p.
121. **Marko Eltermann**. Analysis of samarium doped TiO_2 optical and multi-response oxygen sensing capabilities. Tartu, 2019, 113 p.